iScience

Article

Molecular differences between young and mature stria vascularis from organotypic explants and transcriptomics

Graphical abstract

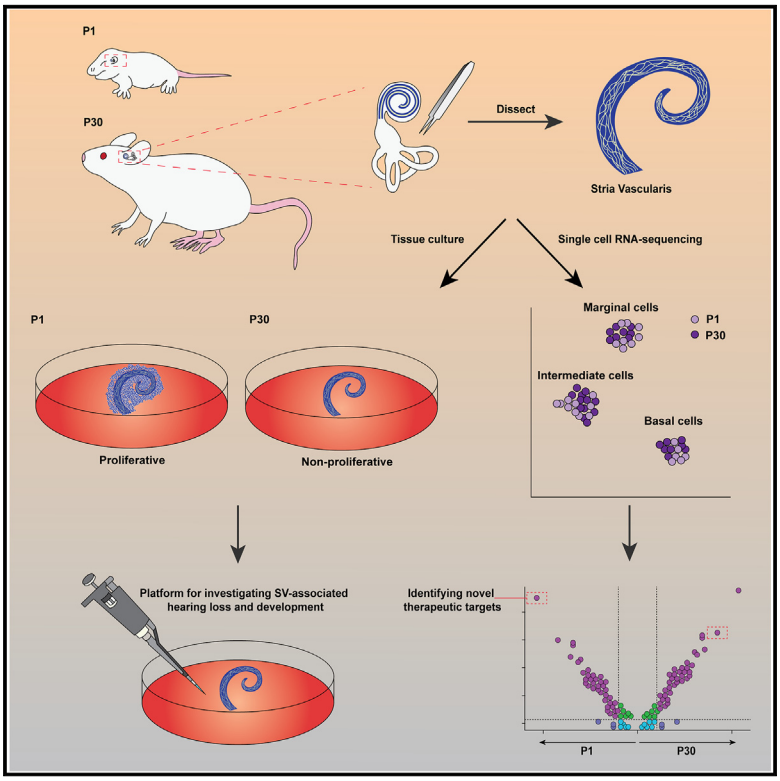

Highlights

- Established an organotypic explant system of young and mature SV with an intact BLB
- *In vitro* proliferation of the SV decreases with age, modeling its behavior *in vivo*
- *In vitro* inhibition of Wnt signaling decreases proliferation in the young SV
- Genes unique to young and mature SV were revealed using single-cell RNA sequencing

Authors

Matsya Ruppari Thulasiram, Ryosuke Yamamoto, Rafal T. Olszewski, Shoujun Gu, Robert J. Morell, Michael Hoa, Alain Dabdoub

Correspondence

adabdoub@sri.utoronto.ca

In brief

Biochemistry; Clinical anatomy; Transcriptomics

Thulasiram et al., 2025, iScience *28*, 111832
February 21, 2025
https://doi.org/10.1016/j.isci.2025.111832

CellPress

iScience

CellPress
OPEN ACCESS

Article

Molecular differences between young and mature stria vascularis from organotypic explants and transcriptomics

Matsya Ruppari Thulasiram,[1] Ryosuke Yamamoto,[2] Rafal T. Olszewski,[3] Shoujun Gu,[3] Robert J. Morell,[4] Michael Hoa,[3,5] and Alain Dabdoub[1,2,6,7,*]

[1]Department of Laboratory Medicine and Pathobiology, University of Toronto, Toronto, ON M5S 1A8, Canada
[2]Biological Sciences, Sunnybrook Research Institute, Sunnybrook Health Sciences Centre Toronto, ON M4N 3M5, Canada
[3]Auditory Development and Restoration Program, NIDCD Otolaryngology-Surgeon-Scientist Program, NIDCD Neurotology Branch, Division of Intramural Research, National Institutes on Deafness and Other Communication Disorders, National Institutes of Health, Bethesda, MD 20892, USA
[4]NIDCD/NIDCR Genomics and Computational Biology Core, National Institutes of Deafness and Other Communication Disorders, National Institutes of Health, Bethesda, MD 20892, USA
[5]Department of Otolaryngology-Head and Neck Surgery, Georgetown University School of Medicine, Washington, DC 20007, USA
[6]Department of Otolaryngology–Head and Neck Surgery, University of Toronto, Toronto, ON M5S 1A8, Canada
[7]Lead contact
*Correspondence: adabdoub@sri.utoronto.ca
https://doi.org/10.1016/j.isci.2025.111832

SUMMARY

The stria vascularis (SV) is an essential component of the inner ear that regulates the ionic environment required for hearing. SV degeneration disrupts cochlear homeostasis, leading to irreversible hearing loss, yet a comprehensive understanding of the SV, and consequently therapeutic availability for SV degeneration, is lacking. We developed a whole-tissue explant model from neonatal and mature mice to create a platform for advancing SV research. We validated our model by demonstrating that the proliferative behavior of the SV *in vitro* mimics SV *in vivo*. We also provided evidence for pharmacological experimentation by investigating the role of Wnt/β-catenin signaling in SV proliferation. Finally, we performed single-cell RNA sequencing from *in vivo* neonatal and mature mouse SV and surrounding tissue and revealed key genes and pathways that may play a role in SV proliferation and maintenance. Together, our results contribute new insights into investigating biological solutions for SV-associated hearing loss.

INTRODUCTION

Hearing relies on the regulation of cochlear homeostasis by the stria vascularis (SV). The SV lines the lateral wall of the inner ear and is composed of three epithelial cell layers (Figures 1A and 1B): the marginal layer originates from the otic epithelium and faces the endolymph of the scala media[1]; the intermediate cell layer is made up of intermediate cells derived from the neural crest[2–6] and a network of endothelial cells and pericytes that make up the blood-labyrinth barrier[7,8] (BLB; Figures 1A and 1B); the basal cells arise from the otic mesenchyme and are connected to the spiral ligament fibrocytes.[9–11] The SV generates and maintains the endocochlear potential that is required for sound transduction and protects the inner ear against pathogenic infiltration, making it crucial for hearing. SV degeneration can occur due to aging, ototoxic drugs, and genetic disease, which can lead to progressive and irreversible hearing loss.[12–18] In these situations, there is no evidence that the SV has endogenous regenerative capacity, and therefore, there is a need to better understand the SV to develop targeted regenerative therapies.

One of the main limitations for advancing SV research is the lack of an *in vitro* system that investigates the SV as a whole tissue. *In vitro* organotypic explants of cochlear and vestibular organs have led to novel discoveries regarding their development and function.[19–21] Systems developed for the SV hold the same potential. Techniques that currently exist for the SV include isolation, purification, and culture of the individual SV or BLB cell types[22–24] or fragmented explant culture.[25–27] Although these methods provide a platform for investigation, they do not examine the SV as a whole tissue. This could lead to an oversight of key information that could contribute to our understanding of the SV and the evaluation of therapies. Recently, single-cell RNA sequencing has allowed for cell-specific characterization of the whole SV in both normal and hearing loss mouse models.[28–32] However, the molecular underpinnings of SV development, maintenance, and degeneration have yet to be fully elucidated.

We sought to provide a deeper understanding of the SV by contributing to the advancement of *in vitro* and bioinformatic studies. Whole-organ explant cultures provide the advantage of preserving architectural and molecular integrity, which can better inform understanding of the organ *in vivo* and allow for

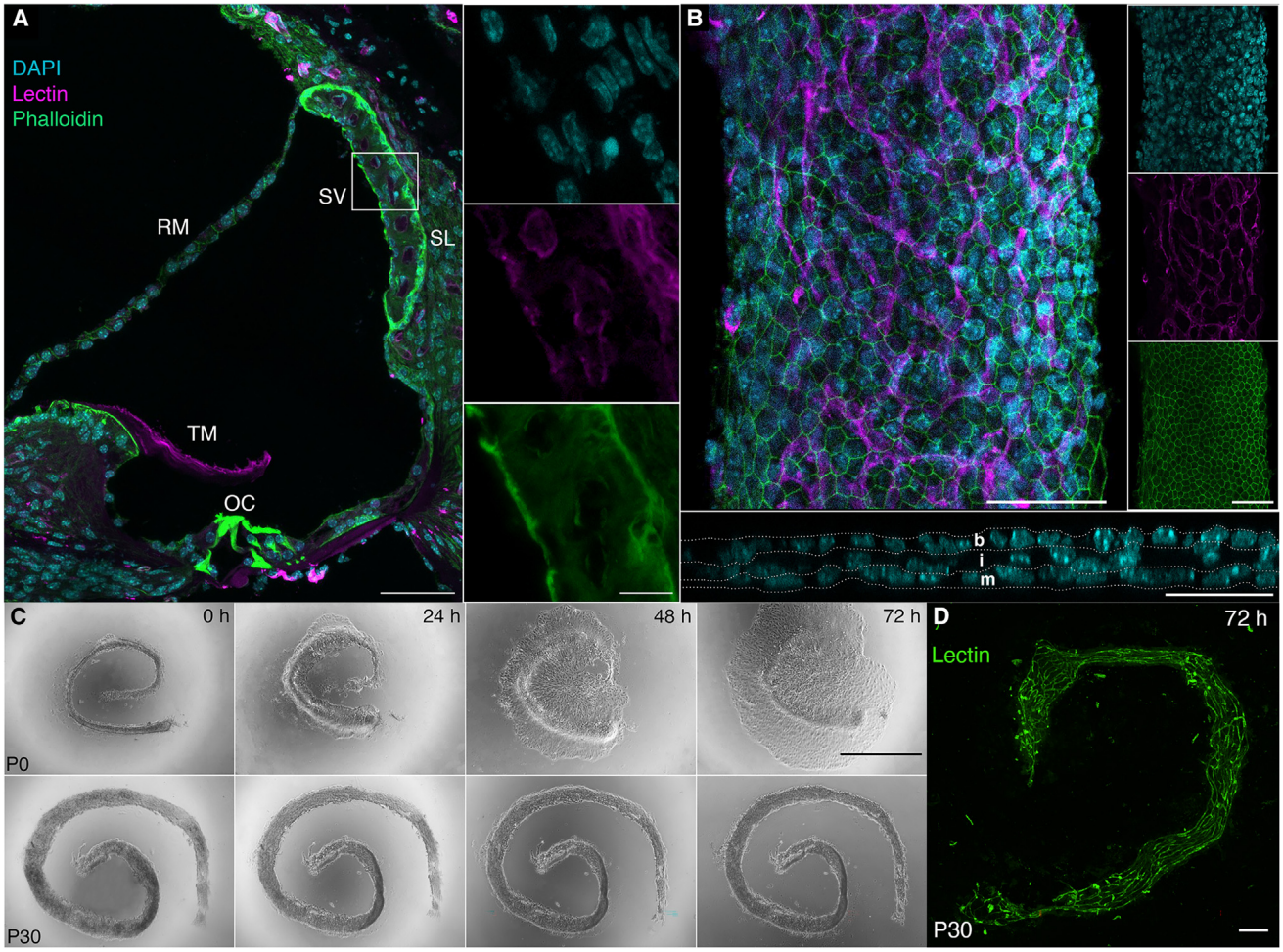

Figure 1. Generating an *in vitro* organotypic explant model for the young and mature mouse stria vascularis

(A and B) P30 cross-section of a cochlear turn (A) and P0 whole-mount stria vascularis (B) stained with Phalloidin for actin (green), lectin for blood vessels (magenta), and DAPI for nuclei (blue). Orthogonal view of the whole-mount SV in bottom panel of (B) marks the nuclei of the three cell layers of the SV (white dashed lines). Scale bars in (A): 50 μm in low-magnification images, 10 μm in high-magnification images. Scale bars in (B): 50 μm.

(C) Side-by-side differential interference contrast imaging of neonatal and adult SV organotypic explants. SV were dissected and cultured on Matrigel-coated plates in standard conditions for 72 h. Scale bar: 1 mm.

(D) Representative image of a P30 SV cultured for 72 h stained with lectin. Scale bar: 200 μm. m, marginal cells; i, intermediate cells; b, basal cells; SV, stria vascularis; SL, spiral ligament; OC, organ of Corti; TM, tectorial membrane; RM, Reissner's membrane.

more comprehensive *in vitro* studies including damage paradigms and therapeutic interventions. Therefore, we developed an organotypic explant model of the SV for both neonatal and functionally mature mice. We showed that our *in vitro* system recapitulated SV proliferation *in vivo* and conducted pharmacological studies using our system, demonstrating a robust, representative, and reproducible model to study the SV. To then understand the transcriptomic landscape of the SV further, we used single-cell RNA sequencing and compared the neonatal and mature SV. We revealed significant differences in gene expression patterns and bioinformatically characterized the proliferative properties of SV cell types. We further identified genes, transcription factors, pathways, and cell-to-cell interactions unique to each stage that may play a role in SV proliferation, development, and maintenance. Overall, our novel experimental platform and single-cell RNA sequencing data provide new knowledge and insights into understanding the SV in the pursuit of developing biological solutions for SV-associated hearing loss.

RESULTS

Establishing an *in vitro* culture model for the SV

The development of a whole-tissue culture model will enable comprehensive studies for the SV and create a platform for testing potential therapeutics. With these goals in mind, we established an organotypic explant culture model using young and functionally mature mice to study the whole SV (Figure 1C). In brief, the three cell layers of the SV and the associated vasculature were dissected from base to apex from P0-P35 CD1 mice

(Figure 1B), and isolation of SV cells was verified through immunohistochemistry and transcriptomics prior to being cultured (Figure S1, data not shown). All stages were cultured on Matrigel-coated plates for 72 h before fixation with 4% paraformaldehyde (PFA). We initially observed that the P0-1 SV had growth and spread of cells, whereas the P30-35 SV did not (Figures 1C and 1D). We hypothesized that this could be a result of cell proliferation, and to assess this, we cultured P0-1 SV for 72 h and exposed the explants to 3.5 μg/mL BrdU for different durations within the culture period and quantified proliferation by calculating the fraction of $BrdU^+$ nuclei among DAPI-stained nuclei (Figures 2A–2D). We detected $BrdU^+$ nuclei within 1.5 h in culture and significant accumulation of BrdU within 24 h [$F(5, 64) = 56.23$, $p < 0.0001$; Figure 2D]. We next investigated which specific SV cell type(s) were proliferating and performed reverse transcription quantitative real-time PCR to compare mRNA expression before and after culturing. Our results indicated that expression of *Kcnq1,* a marker for marginal cells, was significantly lower after 72h in culture, and *Cldn11*, a marker for basal cells, showed no significant difference before and after culture (Figure 2E). However, expression of *Kcnj10* was significantly increased in cultured SV ($p = 0.0215$), suggesting that the main proliferating SV cell types are intermediate cells. This falls in line with previously published work tracking intermediate cell proliferation *in vivo*.[3] Together, our results demonstrated that the P0 SV exhibits active and persistent proliferation *in vitro* and that the intermediate cells are contributing to this effect.

The neonatal SV is highly proliferative *in vitro*, and proliferation decreases during postnatal development

We next determined the proliferative capacity of the SV during postnatal development. We cultured SV from P0-1, P7-8, and P30-35 mice and observed a significant decrease in proliferation as measured by the proportion of $BrdU^+$ cells in relation to DAPI-labeled cells at P7-8 ($p = 0.02$) and P30-35 ($p < 0.0001$) compared to P0-1 (Figures 3A–3D). This indicated that while the SV retains its proliferative capacity at neonatal stages, proliferation decreases with age.

Next, we examined whether the proliferative effect we observed *in vitro* recapitulated the behavior of the SV in the ear. We validated proliferation *in vivo* by immunolabeling for Ki67, an endogenous marker of proliferation[33,34] in cryosections of P0 and P30 mouse cochleae. In agreement with published reports,[3] we observed $Ki67^+$ cells at P0 in the intermediate cell layer near the vasculature but not at P30 (Figures 3E–3F″). Furthermore, using reverse transcription quantitative real-time PCR, we quantified a significant decrease in *Ki67* mRNA expression in P30-35 SV compared to P0-1 SV ($p < 0.0001$; Figure 3G). Taken together, the proliferative behavior of the SV in our *in vitro* model was comparable to *in vivo*, validating our system as a representative experimental platform to investigate the SV.

Wnt/β-catenin signaling plays a role in SV proliferation

We then tested the utility of our *in vitro* system to pharmacological intervention by asking what molecular pathways were driving proliferation in the neonatal SV. A well-known pathway involved in proliferation and angiogenesis is the canonical Wnt/β-catenin (Wnt) signaling pathway.[35] We have previously shown that the canonical Wnt signaling pathway is highly active in the developing cochlea and that activating Wnt signaling at embryonic and postnatal stages promotes proliferation of cochlear supporting cells.[36,37] We have also reported that Wnt signaling components are expressed in the SV.[30,38,39] To examine the role of Wnt signaling in SV proliferation, we used a pharmacological inhibitor of Wnt signaling called FH535 that targets the TCF/LEF transcription factors responsible for regulating downstream Wnt target genes. We administered FH535 at 1, 2.5, 5, and 10 μM for 72 h on P0-1-cultured SV and found that proliferation significantly decreased in cultures treated with 5 μM ($p = 0.0003$) and 10 μM ($p < 0.0001$) FH535 compared to DMSO controls (Figures 4A–4D). These results showed that our culture model is robust to experimentation including pharmacological intervention and indicated that canonical Wnt signaling is at least in part responsible for regulating proliferation in the SV.

Profiling the P1 and P30 transcriptome using single-cell RNA sequencing

To gain a further understanding of the molecular differences between the neonatal and mature SV and their neighboring cell populations, we utilized single-cell RNA sequencing. Here, rather than isolate the SV, we collected surrounding tissue as well to gain comprehensive insight into the molecular interactions between the SV and other cell types of the inner ear. We collected samples from *in vivo* P1 and P30 CBA/J mice and processed them as previously described.[30] We performed unsupervised bioinformatic clustering using Seurat and resolved cluster identity using published cell-type-specific markers.[29,30] We then defined marginal, intermediate, and basal cell clusters in both neonatal and mature SV and validated the expression of cell-type-specific markers in these populations using immunofluorescence (Figures 5A–5C).

To annotate the remaining clusters in our dataset, we integrated P8, P12, and P20 single-cell RNA sequencing data from Jean et al., 2023.[29] We identified root cells (solute carrier family 26 member 4 [*Slc26a4*] and epiphycan [*Epyc*]), spindle cells (*Slc26a4* and annexin A1 [*Anxa1*]), macrophages (adhesion G protein-coupled receptor E1 [*Adgre1*] and macrosialin [*Cd68*]), fibrocytes (otospiralin [*Otos*]), tympanic border cells (elastin microfibril interfacer 2 [*Emilin2*] and palmitoleoyl-protein carboxylesterase [*Notum*]), pre-osteoblasts (RUNX family transcription factor 2 [*Runx2*] and distal-less homeobox 5 [*Dlx5*]), two mixed populations with endothelial and pericyte characteristics (which we labeled fibrocyte [FB]-derived cell 1 and 2; Fms-related receptor tyrosine kinase 1 [*Flt1*], endothelial cell adhesion molecule [*Esam*], platelet-derived growth factor receptor β [*Pdgfrb*], and regulator of G protein signaling 5 [*Rgs5*]), and cells from the surrounding structure (odd-skipped related transcription factor 2 protein [*Osr2*] and chordin-like protein 1 [*Chrdl1*]). We also had three smaller clusters with unknown identity, which we have marked as "unidentified" (Figure 5B; Table S1).

To unveil proliferative differences between the P1 and P30 SV, we identified proliferating cell populations using S.Score and G2M.Score with Seurat, which calculates cell-cycle scores using known markers of S phase and G2/M phase of the cell cycle. We identified that of the three main cell types, a subset of intermediate cells undergo proliferation at P1, which corresponds with the expression of the proliferation marker, *Ki67* (Figure 5D).

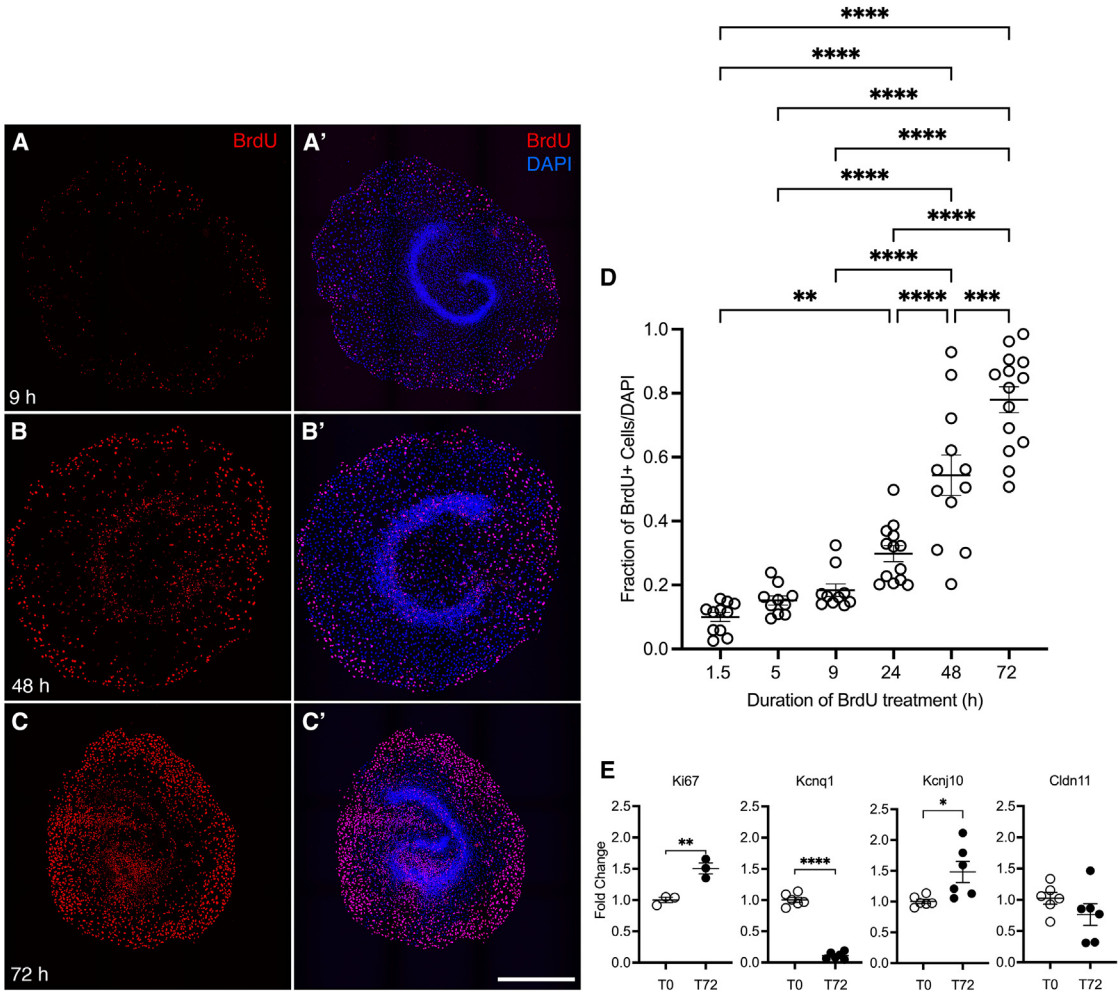

Figure 2. Proliferation of the P0 SV is ongoing throughout 72 h in culture

(A–C) Representative images of P0 SV proliferation across different timepoints over 72 h with the proliferation marker, BrdU (red). (A′–C′) Merged images of BrdU$^+$ nuclei and DAPI stained nuclei (blue). Scale bar: 1mm.

(D) Proliferation quantified as the fraction of BrdU$^+$ nuclei over total DAPI stained nuclei. A one-way ANOVA was performed, $F(5, 64) = 56.23$, $p < 0.0001$. Tukey's multiple comparisons test was performed for post-hoc analysis. $^{**}p = 0.0044$, $^{***}p = 0.001$, $^{****}p < 0.0001$.

(E) reverse transcription quantitative real-time PCR quantifying expression of SV marker genes directly after harvesting (T0) and 72 h after culture (T72). Individual t tests were performed: Ki67 $t(4) = 5.14$, $^{**}p = 0.0068$; Kcnq1 $t(10) = 19.45$, $^{****}p < 0.0001$; Kcnj10 $t(10) = 2.722$, $^{*}p = 0.0215$; Cldn11 $t(10) = 1.310$. Graphs show mean with SEM.

We then sought to gain a deeper understanding of the specific cell types of the SV and surrounding cells. As fibrocytes are closely associated with basal cells, we were interested in understanding their relationship. Fibrocytes regulate ion homeostasis alongside the SV and play a major role in cochlear blood flow regulation, immune response, and recovery from trauma.[40,41] Fibrocytes proliferate after injury even in adult animals,[42,43] which makes them a very interesting candidate population to study lateral wall regeneration. We performed a pseudotime analysis and identified a clear trajectory of cell development from the fibrocytes to the basal cells from P1 to P30 (Figure 6A; Figure S2). We analyzed the top 300 genes along the trajectory to further understand the transitional process of basal cell development. In accordance with previous reports,[11] we identified some genes that are involved in mesenchymal-to-epithelial transition of the fibrocytes into basal cells: expression of *Vim* (vimentin), a mesenchymal marker, decreased along pseudotime, whereas the expression of *Cdh1* (E-cadherin), an epithelial marker, increased (Figure 6B). We also identified that expression of the gap junction protein genes, *Gjb2* (connexin 26) and *Gjb6* (connexin 30), increased in basal cells compared to fibrocytes, and expression of several genes from the collagen families decreased (Figure 6B). Mutations of *Gjb2* and *Gjb6* are associated with the most common autosomal recessive hereditary hearing loss, and deficiencies in one or both genes can cause significant reduction of the endocochlear potential.[44,45] Collagen plays an important role in the spiral ligament (SL) as it helps form the extracellular matrix[46] and thereby maintains the structural integrity of the lateral wall. Thus, our pseudotime analysis provides a molecular landscape of the distribution of functional genes that both distinguish and conjoin the SV and the SL.

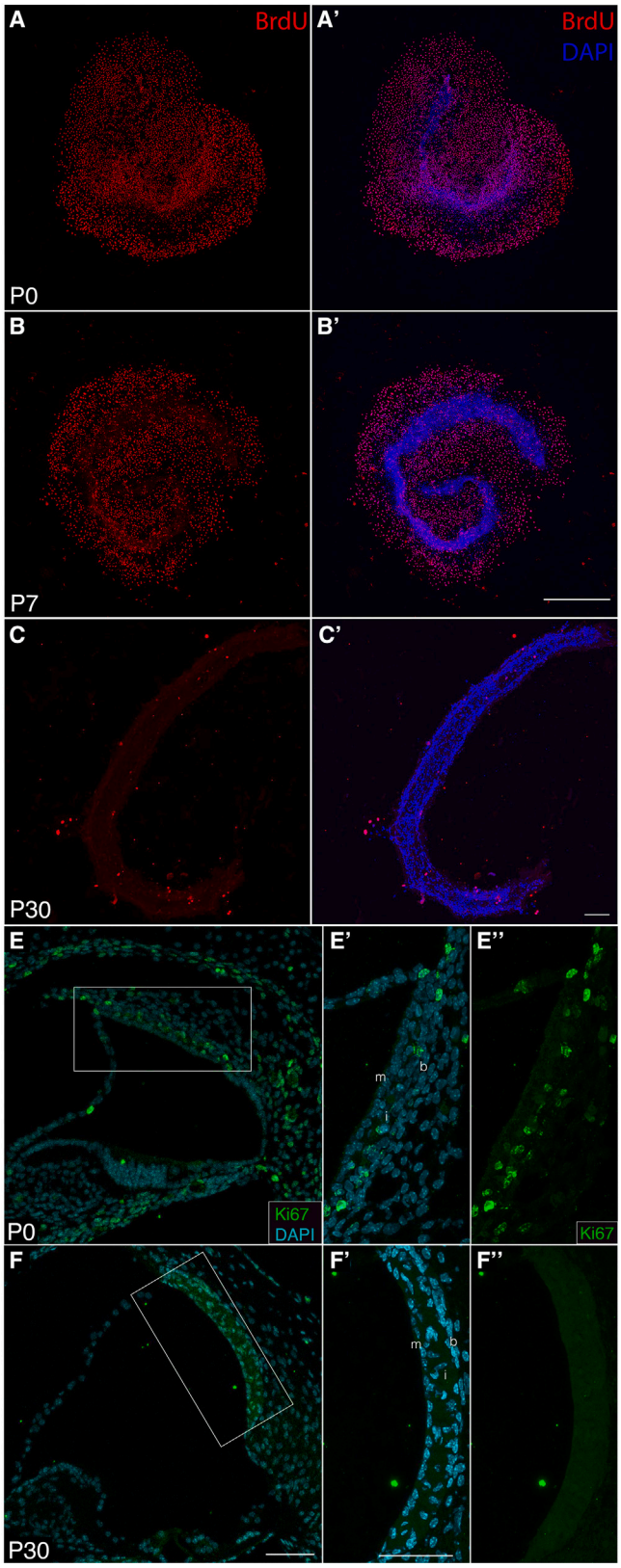

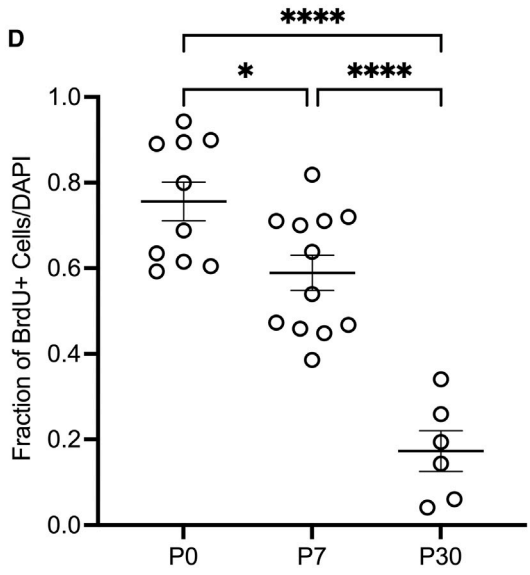

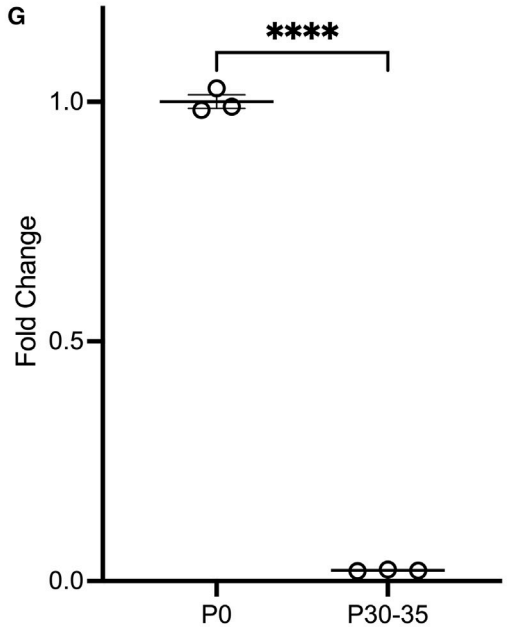

(legend on next page)

We further characterized the intermediate cells of the SV, as their exact identity is unclear. Although there is evidence showing that intermediate cells share melanocyte and macrophage characteristics,[27,47,48] intermediate cells have been widely classified as solely melanocytes. They arise either directly from the neural crest, or indirectly from Schwann cell precursors, which are a population of neural crest cells that emigrate to the peripheral nerve early in development.[49–51] A majority of intermediate cells are derived from Schwann cell precursors.[3,51] We subclustered the intermediate cell population to determine if we could identify these two populations. Here, we identified two subclusters of intermediate cells, which we labeled subcluster_0 and subcluster_1 (Figures 7A and 7B). GO biological process terms associated with subcluster_0 included cellular localization and anatomical structure development, whereas subcluster_1 included oxidative phosphorylation and generation of precursor metabolites and energy (Figure 7C). Interestingly, our data showed that marker genes for subcluster_0 include many, if not all, of the recognized canonical markers of intermediate cells, including *Kcnj10* (potassium inwardly rectifying channel subfamily J member 10), *Met* (met proto-oncogene), *Dct* (dopachrome tautomerase), and *Plp1* (proteolipid protein 1), as well as non-canonical markers such as *Col5a3* (collagen type V alpha 3 chain; Table S2). Genes upregulated in subcluster_1 include *Vegfb* (vascular endothelial growth factor B), *Scn1b* (sodium voltage-gated channel beta subunit 1), *Mt1* (metallothionein 1), and *Ldha* (lactate dehydrogenase A; Table S2). We validated *Col5a3* and *Ldha* as candidate genes per subcluster using RNAscope, along with *Kcnj10* and *Plp1* as our known marker genes (Figures 7D–7E′). Although more investigation is required, these results may begin to elucidate the molecular identity of the intermediate cell subtypes and their origins.

Differential gene expression analysis reveals transcriptional differences between the P1 and P30 SV

To examine the transcriptional differences between the young and mature SV, we performed differential gene expression analysis comparing the P1 to P30 SV for marginal, intermediate, and basal cells (Figures 8A–8C). We were particularly interested in genes that were uniquely upregulated at either P1 or P30 or in one specific cell type. Among the top significantly enriched genes in P1 marginal cells, the ion channels *Dpp10* (dipeptidyl peptidase 10) and *Cacnb2* (calcium voltage-gated channel auxiliary subunit beta 2) were unique to this cluster. *Dpp10* is a potassium channel ancillary subunit and is known to associate with the voltage-gated potassium channel family Kv4,[52] and *Cacnb2* has been previously reported in the inner hair cells and is required for normal development and hearing function.[53] Similarly, in P1 intermediate cells, the ion channel *Trpm1* (transient receptor potential cation channel subfamily M member 1) and the melanocyte-specific transmembrane protein *Pmel* (premelanosome protein) were upregulated. We validated the differential expression of *Dpp10* and *Trpm1* in P1 and P30 SV sections using RNAscope and found that *in vivo* expression patterns correspond with our bioinformatic results (Figures 8D–8E′). We further examined transcription factors that were differentially expressed between P1 and P30 in each cell type. There were fewer transcription factors expressed at P30 than at P1 in marginal and intermediate cells but not basal cells. We again observed genes that were uniquely upregulated. For example, *Dach1* and *Meis1* are two transcription factors only enriched in P1 marginal cells, and they have been previously known to be involved in regulatory processes of the SV.[54,55] Table 1 provides a complete list of all significant uniquely expressed genes, including transcription factors and cofactors, expressed at each age and cell type.

We also performed functional enrichment analysis using gProfiler, using all significantly upregulated genes at P1 and P30 in marginal, intermediate, and basal cells. We ran independent analyses for each cell type at each stage and observed that the top 20 enriched gene Ontology (GO) terms for biological processes in P1 were widely associated with development, whereas at P30 they were associated with SV function and maintenance (Figures 8A–8C; Table S3). Terms associated with proliferation and differentiation were identified at P1: cell population proliferation (GO:0008283) in marginal and intermediate cells, cell differentiation (GO:0030154) in marginal and basal cells, neuron differentiation (GO:0030182) in intermediate cells, and cell migration (GO:0016477) in basal cells. Collectively, differential gene expression analysis coupled with functional enrichment analysis of single-cell transcriptomes from both the proliferative neonatal and non-proliferative mature SVs enabled a more comprehensive examination of the changes underlying SV development.

CellChat examines cell-cell communication and ligand-receptor interactions at P1 and P30

The previous analyses provided an understanding about cellular identity within the specific populations at young and mature stages. To gain further insight into cell-cell interactions, we performed CellChat analysis. We revealed several pathways involved in forming the extracellular matrix, cell proliferation, and differentiation and maintaining tissue structural integrity (Figure 8F). We observed that cell-cell interaction patterns and pathway signaling strength differed between the P1 and P30: in many cases, at P1, a signaling pathway was expressed in several different cell types, whereas at P30, expression becomes more specified to fewer cell types. We also identified some

Figure 3. Proliferation of the stria vascularis decreases with age

(A–C) Representative images of organotypic stria vascularis explants at P0, P7, and P30 cultured with the proliferation marker, BrdU (red), over 72 h. (A′–C′) Merged images of $BrdU^+$ nuclei and DAPI-stained nuclei (blue). Scale bars: 1 mm in (A–B′); 200 μm in (C and C′).

(D) Quantification of $BrdU^+$ nuclei. A one-way ANOVA was performed, $F(2, 25) = 34.15$, $p < 0.0001$. Tukey's multiple comparisons test was performed for post-hoc analysis.

(E and F′) Cryosections of the basal turn of the P0 and P30 cochlea were stained with Ki67 (green), Lectin (magenta), and DAPI. Scale bars: 100 μm for low-magnification images; 50 μm in high-magnification images. m, marginal cells; i, intermediate cells; b, basal cells.

(G) Quantification of Ki67 in P0 and P30 SV using reverse transcription quantitative real-time PCR. A two-tailed unpaired t test was performed, $t(4) = 70.16$, $p < 0.0001$. $^*p = 0.0235$, $^{****}p < 0.0001$. All graphs show mean with SEM.

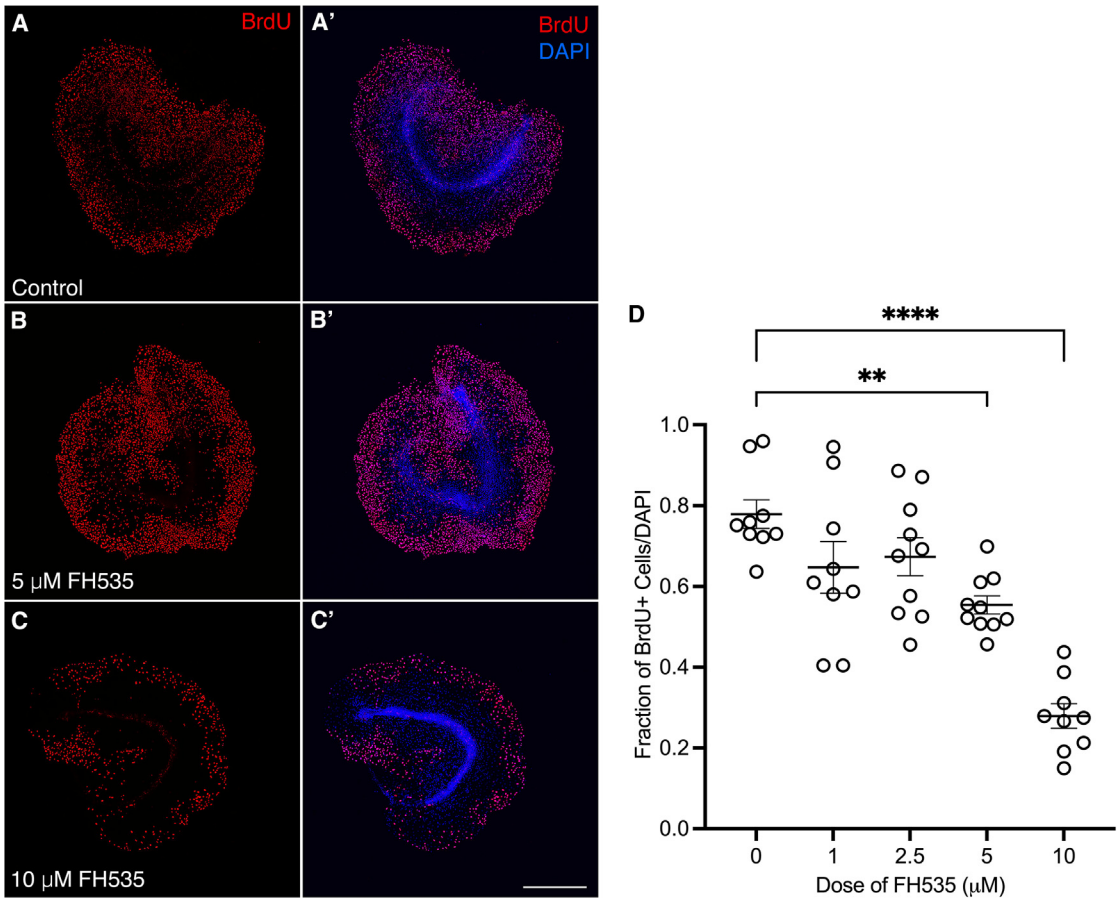

Figure 4. Inhibition of Wnt/β-catenin signaling significantly reduces proliferation of the neonatal stria vascularis

(A–C) Representative images of organotypic P0-P1 stria vascularis explants cultured with either DMSO (control) or FH535, in the presence of BrdU (red) over 72 h. (A′-C′) Merged images of BrdU$^+$ nuclei among DAPI-stained nuclei (blue) in control and FH535-treated cultures. Scale bar: 1 mm.

(D) Quantification of BrdU$^+$ nuclei among DAPI. A one-way ANOVA was performed, $F(4, 42) = 19.74$, $p < 0.0001$. Tukey's multiple comparisons test was performed for post-hoc analysis. $^{**}p = 0.004$, $^{****}p < 0.0001$. Graph shows mean with SEM.

pathways that are specific to P1 and P30, for instance, Vcam signaling at P1 and Tweak signaling at P30. Tables S4 and S5 describe all ligand-receptor interactions at both stages.

At P1, the top five signaling pathways were Collagen, Ptn (pleiotrophin), Mk (midkine), Epha, and Cldn (claudin) and at P30, they were Ptn, Cldn, Mk, Spp1 (secreted phosphoprotein-1), and Psap (prosaposin). Some proteins, such as collagen and claudin, have been studied in the SV. Collagens are important extracellular matrix proteins that maintain the structural integrity of the SV,[56–58] and Cldn (Claudins) are cell adhesion proteins that maintain the SV by regulating tight junctions.[59,60] There is considerably less information regarding Ptn, Mk, Spp1, and Psap. Ptn is an evolutionarily conserved neurotrophic factor that shares homology with Mk and regulates developmental and angiogenic processes.[61] *Ptn* or *Mk* knockout in mice leads to a lack of Kir4.1 expression in intermediate cells.[62] Epha is a receptor tyrosine kinase belonging to the ephrin receptor subfamily.[63] Spp1 is a signaling protein that plays a role in immune function in disease.[64] In the inner ear *Spp1* has been previously characterized as a type I vestibular hair cell marker and more recently identified in cisplatin-treated SV.[32,65] Finally, Psap is precursor protein to the sphingolipid activator protein family (saposins) and is a secreted neuro- and glio-protective protein.[66] Prosaposin has been identified in the organ of Corti of rats and mice[67] and in the basal cells of the rat SV.[68] *Psap* knockout mice show impaired hearing[67] but more investigation is required to understand its role in the SV. Cell-cell communication analysis of the SV at young and mature stages has provided more information about the intricate interactions within the SV and has revealed pathways that may have been previously overlooked.

DISCUSSION

The goal of this study was to one, provide an accessible platform to study the SV, and two, provide a comparative profile of the molecular differences between the young and mature SV. We used whole-organ *in vitro* explants of P0-P35 SV to show the proliferative differences throughout postnatal development, and we used single-cell RNA sequencing to further compare the transcriptome profiles of young vs. mature SV.

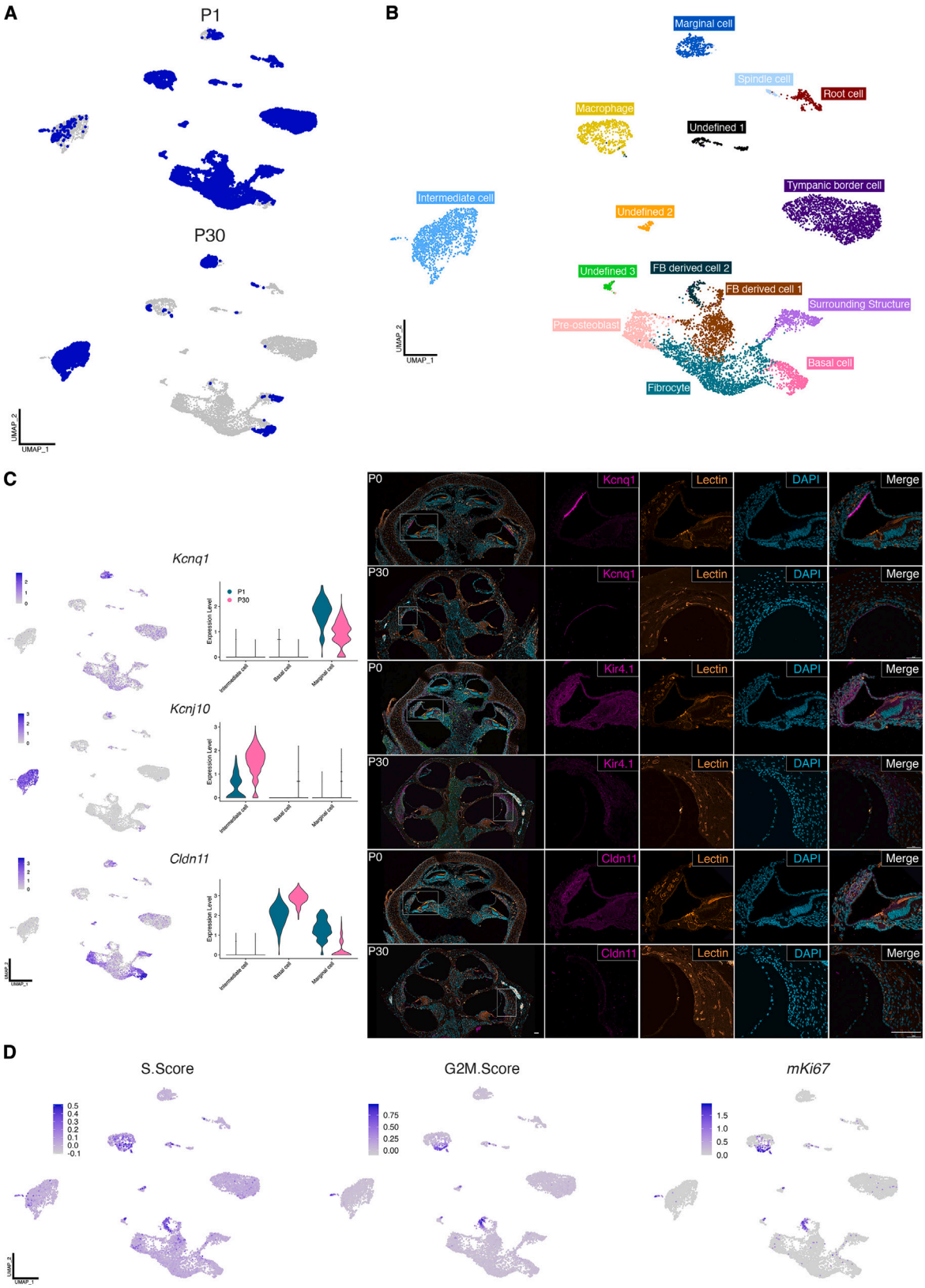

(legend on next page)

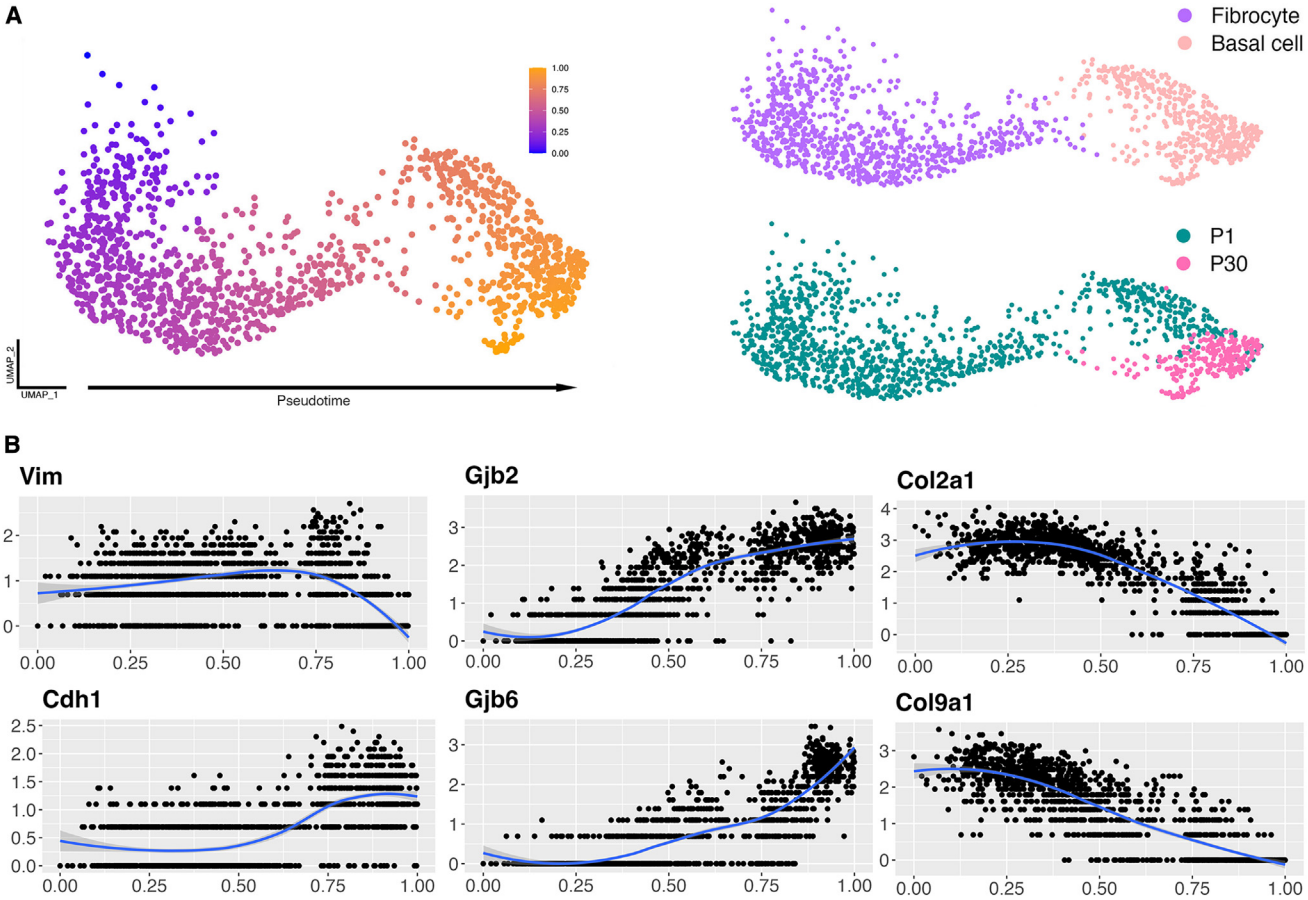

Figure 6. Pseudotime analysis shows a developmental trajectory from fibrocytes to basal cells

(A) Pseudotime analysis showing fibrocyte to basal cell trajectory, and UMAPs displaying fibrocyte and basal cell subclusters and sample stage distribution.

(B) Expression of different genes in fibrocytes and basal cells along pseudotime.

Our comprehensive analyses provide in-depth insights into the molecular composition of the SV and reveal genes and pathways that contribute to SV-associated hearing loss pathologies.

We are the first to culture whole SV in both neonatal and functionally mature mice. The inner ear is difficult to access due to its deep location in the skull and encapsulation in dense bone. The advent of inner ear organotypic explants overcame this challenge when studying other inner ear cell types.[19–21] Organotypic explants of the SV hold the same potential for discovery. One advantage of our protocol is that we preserve the cellular architecture of the SV to study the interactions between cell types along the basal-to-apical axis of the tissue. Our system can potentially be used to investigate different biological pathways involved in SV development, regulation, and disease, compare age-related differences in the SV, as well as test the effectiveness and bioavailability of therapeutic candidates.

We investigated SV proliferation *in vitro* using the thymidine analog, BrdU, and *in vivo* using Ki67. Consistent with previous reports using neonatal fragmented SV cultures, we observed proliferative cells that migrated out from the explanted neonatal tissue.[26] We identified the proliferative cells as intermediate cells and observed that their proliferation declines during postnatal development, consistent with reports from Renauld et al., 2022.[3] We identified that a molecular mechanism regulating SV proliferation was Wnt/β-catenin signaling, which is a prominent pathway involved in proliferation.[35,69] Wnt/β-catenin signaling is initiated when Wnt ligands bind to Frizzled receptors and Lrp5/6 co-receptors. This triggers the events that lead to the

Figure 5. Annotation of cell types and proliferative clusters in P1 and P30 single-cell RNA sequencing data

(A) UMAP showing P1 and P30 SV single-cell RNA sequencing sample distribution among 15 cell clusters.

(B) Integrated and annotated UMAP of cell types acquired through single-cell RNA sequencing P1 and P30 SV.

(C) UMAPS and violin plots of candidate marker genes for marginal, intermediate, and basal cells. Immunohistochemical validation of candidate marker genes in cryosections of P0 and P30 cochleae. Scale bars: 100 μm for low-magnification images; 50 μm for high-magnification images.

(D) UMAPs showing clusters in which cells undergo proliferation.

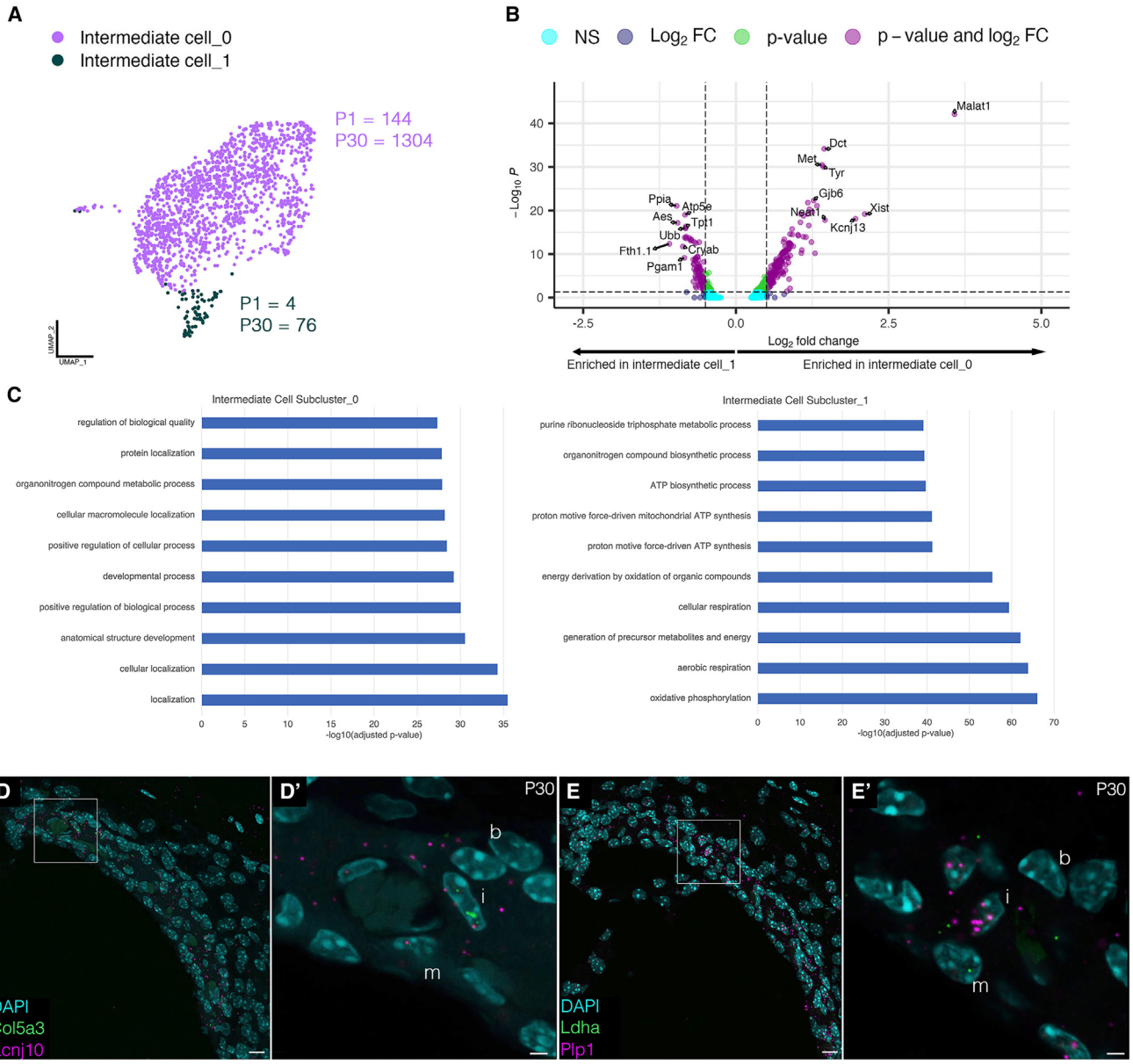

Figure 7. Intermediate cell clustering reveals two subtypes of intermediate cells

(A) UMAP displaying intermediate cell subclusters with the distribution of P1 and P30 cells annotated and (B) volcano plot showing differential gene expression between subclusters.

(C) Bar graphs depict top 10 GO biological processes (bottom left and right).

(D and E′) Representative images of RNAscope validation of intermediate cell_0 and _1 genes. m, marginal cells; i, intermediate cells; b, basal cells. Scale bars: 10 μm in (D and E) and 2.5 μm in (D′ and E′).

accumulation and subsequent translocation of intracellular β-catenin to the nucleus. Nuclear β-catenin then binds to the TCF/LEF transcription factors to activate the transcription of downstream Wnt target genes. We showed that inhibiting TCF/LEF transcription factors results in a significant decrease in proliferation in neonatal cultures, indicating that the Wnt/β-catenin signaling pathway plays a role in the proliferation of the SV. This suggests that Wnt/β-catenin signaling may be a therapeutic target for regenerative SV therapies.

Differential expression analysis revealed the transcription factor *Dach1* to be upregulated in P1 marginal cells. Embryonic shRNA-regulated knockdown of *Dach1* results in a loss of intermediate cells, decreased endocochlear potential, and decreased hearing function in adulthood.[54] These results suggest that *Dach1* may be an important regulator of SV development. It also suggests that the association between marginal and intermediate cells may be an important factor in SV development. In accordance with this, we observed the upregulation of *Spp1*

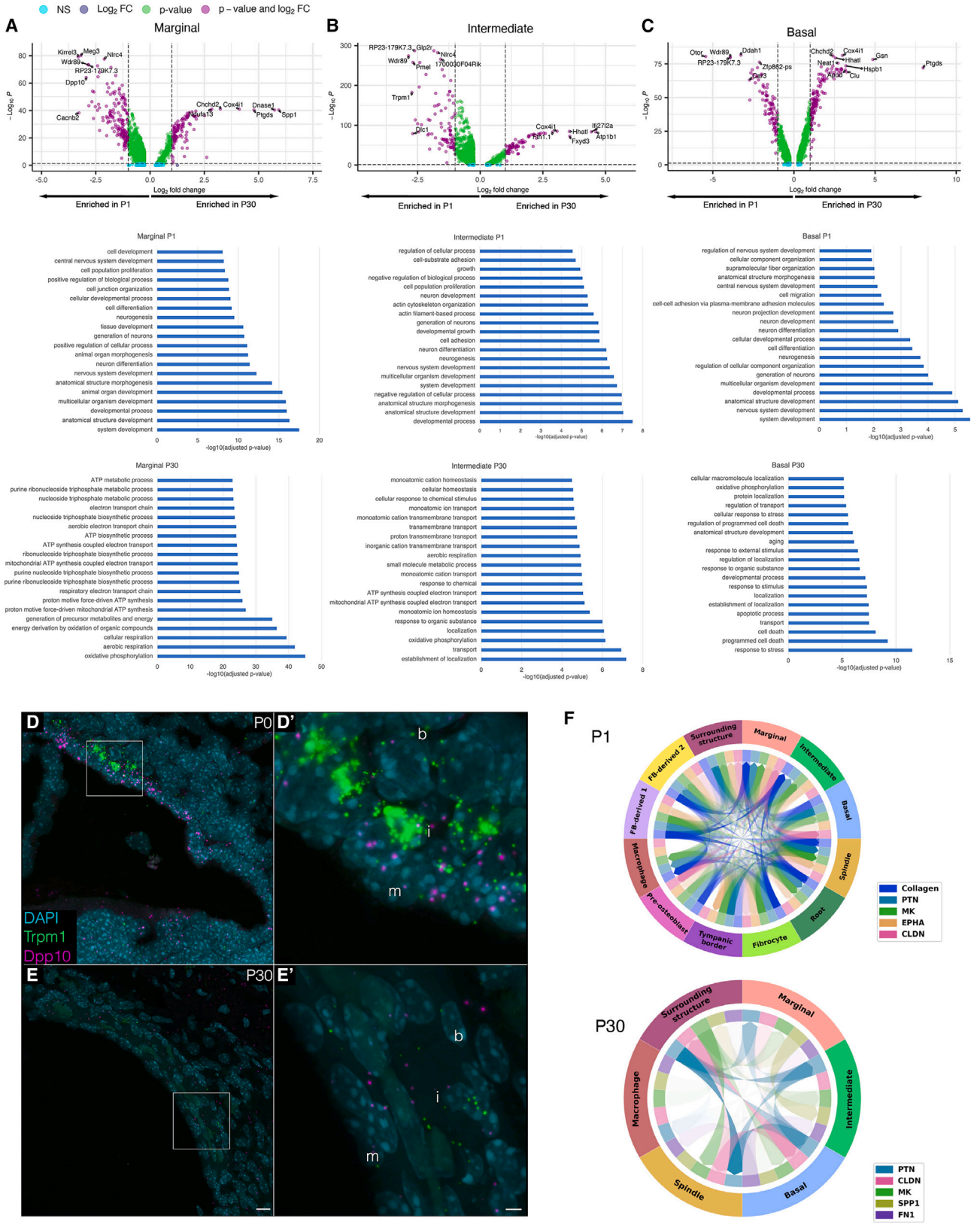

(legend on next page)

(secreted phosphoprotein 1) in P30 marginal and intermediate cells. *Spp1* has been characterized as a vestibular type I hair cell marker using single-cell RNA sequencing.[65] In the SV, the protein encoded by *Spp1*, osteopontin, is highly localized in the marginal cells and secreted into the cochlear fluids.[25,70] Interestingly, *Spp1* is downregulated in the marginal cells of adult mice that have been treated with cisplatin, an ototoxic chemotherapeutic.[32] These observations coupled with our data suggest that *Spp1* may be a candidate gene to investigate SV and endocochlear potential development and is a therapeutic target for cisplatin-induced degeneration of the SV and hearing loss.

Meniere's disease is another disorder that affects the SV. Meniere's disease is a rare inner ear disorder characterized by endolymphatic hydrops and results in vertigo, tinnitus, and hearing loss. The etiology of Meniere's disease is unclear. We observed that the TWEAK signaling pathway is upregulated in the P30 SV, and studies suggest that it may be a potential therapeutic target for Meniere's disease. TWEAK (tumor necrosis factor-like weak inducer of apoptosis) is a member of the tumor necrosis factor superfamily and is a cytokine that has multiple functions in the body, including in inflammation, bone remodeling, angiogenesis, cellular adhesion, proliferation, differentiation, and apoptosis.[71–73] A study examining bilateral Meniere's disease identified that a majority of patients carried a single nucleotide variant rs4947296, which regulates the TWEAK/Fn14 signaling pathway.[74] TWEAK/Fn14 signaling in individuals carrying the variant lead to the activation of both the canonical and non-canonical nuclear factor κB (NF-κB) pathways with downstream inflammatory effects. Although TWEAK signaling was identified to be a candidate therapeutic target for individuals carrying the variant, it was unclear where the site of inflammation was in the ear.[74] Our CellChat data suggest that the TWEAK signal is sent from the intermediate cells, and the receptor is located on the marginal cells and the spindle cells. More information is needed to elucidate the role TWEAK signaling plays in the SV, and it is important to mention that CellChat interactions across sample stages may be a reflection of differences in cell capture and sequencing depth. However, these methods bring us one step closer to pinpointing the pathways involved in multifaceted disorders such as Meniere's disease, and the ligand-receptor interactions between the cell types can facilitate the development of effective therapies.

Identification of genes and pathways of interest also provides more insight into the characterization of each SV cell type. We were most interested in the intermediate cells because of their multifaceted characteristics and their dual embryonic origin. Intermediate cells are primarily defined as melanocytes, although there are few reports that they also exhibit macrophage characteristics.[22,47,48] Melanocytes are reported to originate either directly from the neural crest or from a subset of early delaminated neural crest cells called Schwann cell precursors.[49–51] From the neural crest, or nerve-derived Schwann cell precursors, melanoblasts form and migrate to their desired location in the body and form region-specific melanocytes depending on signaling pathways in the environment, such as KiT/Kitl, Et3/Ednrb, c-MET, and Pax3.[2,6,49,50,75–78] Intermediate cells of the SV derive from these two embryonic populations,[3,51] yet the exact nature of the two intermediate cell populations remains to be distinguished. We found two subclusters of intermediate cells and observed that the canonical markers for intermediate cells were all upregulated in only one subcluster (subcluster_0). The upregulation of *Plp1* in this subcluster suggests that it is derived from Schwann cell precursors, and consistent with Bonnamour et al.,[51] we identified that the majority of intermediate cells encompassed this subpopulation. The second subcluster we identified was much smaller and showed an upregulation of genes involved in metabolic processes, such as *Idh3B* (isocitrate dehydrogenase [NAD(+)] 3 non-catalytic subunit beta), *Urod* (uroporphyrinogen decarboxylase), *Acot13* (acyl-CoA thioesterase 13), and *Rhoa* (Ras homolog family member A). The SV is the energy generator for the inner ear and is therefore highly metabolically active.[16,79] Our data suggest that a subset of intermediate cells is specifically dedicated toward maintaining these processes, providing a clearer distinction between the intermediate cell populations and a better understanding of the functional SV.

Overall, our *in vitro* studies and single-cell RNA sequencing provide a comprehensive understanding of the molecular landscape of the SV. By developing a whole-organ system to culture the young and mature SV, we open the door for more comprehensive studies to investigate the SV in development, disease, and aging. Genes and pathways of interest revealed through single-cell RNA sequencing can be further investigated using this platform to develop biological therapies for SV-associated hearing loss.

Limitations of the study

A limitation of our study was that we were not able to capture endothelial cells or pericytes in our single-cell sequencing study, which are components of the BLB. Wnt signaling, particularly Frizzled-4 signaling, in endothelial cells is crucial for regulating vascular development and maintenance in the brain and the retina,[80] and Frizzled-4 knockout mice experience vascular degeneration in these tissues as well as the inner ear.[81] In fact, dysregulation of the canonical Wnt/β-catenin pathway is the cause of Norrie disease, a progressive vascular disorder that results in hearing loss.[12,15,82] Since we dissect the whole SV including all the components of the BLB for our *in vitro* cultures, it would be pertinent in future work to gain a molecular perspective on the vascular cells of the SV.

Figure 8. Differential expression and CellChat analyses reveal molecular differences between P1 and P30 SV

(A–C) Differential gene expression analysis (volcano plots on the top) and GO biological processes (bar plots on the bottom) determined from P1 and P30 SV in marginal cells, intermediate cells, and basal cells.

(D and E′) Representative images of RNAscope validation of genes differentially expressed between P1 and P30 SV. Scale bars: 10 μm in (D and E) and 2.5 μm in (D′ and E′). m, marginal cells; i, intermediate cells; b, basal cells.

(F) Circos plots from CellChat analysis displaying top five pathways and interaction patterns in P1 and P30 cell types.

Table 1. Unique differentially expressed genes in P30 vs. P1 SV cell types

Marginal P1	Marginal P30	Intermediate P1	Intermediate P30	Basal P1	Basal P30
Cacnb2	*Ube2s*	*Trpm1*	*Bsg*	*Car3*	*Slc2a1*
Meg3	*Abca2*	*Dlc1*	*Herpud1*	*Slit2*	*Hist1h2bc*
Dpp10	*Churc1*	*Pmel*	*Sdc4*	*Grid2*	*Cdkn1a*
Dach1	*Ndufv2*	*Aff3*	*St6galnac2*	*Nav3*	*Bag1*
Meis1	*Slc25a3*	*Chsy3*	*Car2*	*Syt1*	*Selm*
Malat1	*Nme1*	*Ptma*	*Hsp90b1*	*Vim*	*Rhoc*
Ror1	*Mettl26*	*H2afz*	*Thrsp*	*Sema6a*	*Tspan15*
Oc90	*Qsox1*	*Glp2r*	*Alpl*	*Slc1a3*	*Ubxn1*
Sparc	*Sepp1*	*Cdk2*	*Jam2*	*Eef1g*	*Srgn*
Tuba1a	*Ubl5*	*St6galnac3s*	*Atp6ap2*	*Col9a3*	*Plin4*
Slit3	*Igfbp7*	*Sdk1*	*Ctsb*	*Mllt3*	*Tns1*
Sptssa	*Clstn1*	*Opcml*	*Psap*	*Tenm2*	*Gng11*
Sulf1	*Ndufb10*	*Fstl4*	*Atp6v0b*	*Igfbp2*	*Tmem256*
Aldh1a2	*Ndufb11*	*Celf2*	*Sparcl1*	*Fam19a1*	*Lctl*
Kctd8	*Arf5*	*Pfn1*	*Aldh2*	*Igfbp4*	*Kif5b*
Fos	*Atp5c1*	*Ptprm*	*Emp3*	*Itih5*	*Gabarapl2*
Cdh18	*Ndufb2*	*Rap2b*	*Col5a3*	*Nckap5*	*Anxa3*
Btg2	*Cox7b*	*Cfl1*	*Slc45a2*	*Cacna2d3*	*Mrps6*
Exoc6b	*Cox7a2*	*Hmgn1*	*Hspa5*	*Anks1b*	*Hspa1a*
Slc2a13	*Atp5b*	*Actb*	*F3*	*Ebf1*	*Perp*
Naaladl2	*Cd59a*	*Wbp5*	*Xist*	*Lrp4*	*Cited4*
Ppp2r2b	*Sorl1*	*H3f3a*	*Pla2g7*	*Large*	*Mt1*
Ccdc3	*Itpr2*	*Ybx1*	*Gsta2*	*Mdga2*	*Taldo1*
Erc1	*Smpdl3a*	*Hmgn2*	*C2*	*Map7*	*Srebf1*
Dach2	*Mrpl33*	*Sox5*	*Kcnj10*	*Ccdc141*	*Trp53i11*
Cdon	*Cox5a*	*Dip2c*	*Fxyd1*	*Hnrnpa1*	*Hist1h1c*
Add2	*Uqcrc1*	*Tenm4*	*Tmem176b*	*Pip5k1b*	*Bri3*
Esrrb	*Mpc2*	*Phyhipl*	*Scn1b*	*Snrpg*	*Smim14*
Ccser1	*Ndufv1*	*Sox4*	*Tmem176a*	*Ppic*	*Ctsl*
Pard3b	*Prdx5*	*Gas7*	–	*Cytl1*	*Ddx3x*
Tox	*H2-K1*	*Itga4*	–	*Spag5*	*2200002D01Rik*
Lmx1a	*Fam134b*	*Shc4*	–	*Lypd2*	*Lamp1*
Slc35f1	*Ube2b*	*Bcas3*	–	*Klf12*	*S100a13*
Bpifb3	*Lrp2*	*Bnc2*	–	*Adamts12*	*Pla2g16*
Tmtc2	*Paqr5*	*Cox7c*	–	*Col9a2*	*Rapgef3*
Stac	*Atp5j*	*Dock1*	–	*2610203C20Rik*	*Tspan8*
Ldlrad3	*Prom2*	*Nudt16L1*	–	*Clstn2*	*Cd82*
Nfia	*Mt3*	*Atxn1*	–	*Snhg8*	*Ppia*
Bmpr1b	*Ndufs7*	*Thsd7a*	–	*2700069I18Rik*	*Plpp3*
Sgcd	*Ndufb9*	*Rapgef4*	–	*Tspan5*	*Atp1a2*
Dynll1	*Atp5j2*	*Sumo2*	–	*Rgs6*	*Slc5a3*
Junb	*Ndufa5*	*Plekha7*	–	*Grip1*	*Cd63*
Fgfr2	*Rtn4*	*Spg21*	–	*Cntn3*	*Actg1*
Ier2	*Scp2*	*Adam10*	–	*Col9a1*	*Sat1*
Pdgfc	*Cox5b*	*St6gal1*	–	*1500015O10Rik*	*Pou3f3*

(*Continued on next page*)

Table 1. ***Continued***

Marginal P1	Marginal P30	Intermediate P1	Intermediate P30	Basal P1	Basal P30
Exoc4	*Trnp1*	*Cdk4*	–	*Coch*	*Anxa5*
Egr1	*Snhg4*	*Rarb*	–	*Dapl1*	*Fam129b*
Thsd4	*Pkm*	*Oaz1-ps*	–	*Eif3f*	*Tsc22d3*
Pitpnc1	*Ndufa4*	–	–	*Cacna1e*	*Insig1*
Ghr	*Mdh1*	–	–	*Arhgap28*	*Acsl3*
Frmd5	*Hspa4l*	–	–	*Pcdh9*	*Cd81*
Cacnb4	*Hspa1b*	–	–	*Pdzrn3*	*Atp1b3*
S100a11	*Pgam1*	–	–	*A930011G23Rik*	*Skp1a*
Ank3	*Tspan1*	–	–	*Tcf7l1*	*Arhgap29*
Fut9	*Ndufb8*	–	–	*Adgrl3*	*Glul*
Kcnip4	*Ndufs6*	–	–	*Macrod2*	*Cystm1*
Ext1	*Lrpap1*	–	–	*Tmem117*	*Cebpb*
Samd12	*Etnppl*	–	–	*Wwox*	*Fat2*
Kcnq1	*Reep5*	–	–	*Eif3s6-ps1*	*Qpct*
Cldn4	*Alcam*	–	–	–	*Enah*
Ly6e	*Etfb*	–	–	–	*Ackr3*
Tsc22d4	*Slc41a3*	–	–	–	*Aif1l*
Zswim6	*Atp1b2*	–	–	–	*Efhd1*
Cacna2d1	*Cox7a1*	–	–	–	*Ndrg3*
Arhgef38	*Rgs4*	–	–	–	*Dusp1*
Nkain2	*Bglap3*	–	–	–	*Rnf152*
Fn1	*Tesc*	–	–	–	*Ptms*
Etl4	*Dnase1*	–	–	–	*Actn1*
Rbm39	–	–	–	–	*Xpnpep1*
Frem1	–	–	–	–	*Gstm1*
Cited1	–	–	–	–	*Ahnak*
Oxr1	–	–	–	–	*Morf4l1*
2610035D17Rik	–	–	–	–	*Eif1*
Fgf13	–	–	–	–	*Jund*
Sik3	–	–	–	–	*Ephx1*
Nhsl1	–	–	–	–	*Ctxn3*
BC006965	–	–	–	–	*Csrp1*
mt-Atp6	–	–	–	–	*Becn1*
Kansl1	–	–	–	–	*Nudt4*
Pbx1	–	–	–	–	*Isyna1*
Greb1l	–	–	–	–	*Scd1*
Lrba	–	–	–	–	*Ppp1r1a*
Dgki	–	–	–	–	*S100b*
Kcnq1ot1	–	–	–	–	*Apod*
Hbb-bs	–	–	–	–	*Clu*
Chchd3	–	–	–	–	*Gsn*
Fmnl2	–	–	–	–	–
Pax2	–	–	–	–	–
Zbtb20	–	–	–	–	–
Zfr	–	–	–	–	–
Plekhg1	–	–	–	–	–

(*Continued on next page*)

Table 1. *Continued*

Marginal P1	Marginal P30	Intermediate P1	Intermediate P30	Basal P1	Basal P30
Adgrl2	–	–	–	–	–
Cldn6	–	–	–	–	–
Ly6a	–	–	–	–	–
Ppp1r9a	–	–	–	–	–
A830018L16Rik	–	–	–	–	–
Pkp4	–	–	–	–	–
Cited2	–	–	–	–	–
Cox7a2l	–	–	–	–	–
Atrnl1	–	–	–	–	–
Ptk2	–	–	–	–	–
Rcn1	–	–	–	–	–
Pdgfd	–	–	–	–	–
Hipk2	–	–	–	–	–
Fus	–	–	–	–	–
Tuba1b	–	–	–	–	–
Hif1a	–	–	–	–	–
Cirbp	–	–	–	–	–
Ptprd	–	–	–	–	–
Hmcn1	–	–	–	–	–

Significant genes were determined using log2Fc > |1| and Padj <0.05. Transcription factors (single underline) and co-factors (double underline) extracted using AnimalTFDB.

RESOURCE AVAILABILITY

Lead contact

Requests for further information and resources should be directed to and will be fulfilled by the lead contact, Dr. Alain Dabdoub (adabdoub@sri.utoronto.ca).

Materials availability

This study did not generate new unique reagents.

Data and code availability

The single-cell sequencing data generated in these studies have been deposited in the Gene Expression Omnibus (GEO) database (GEO Series accession ID: GSE262019, https://www.ncbi.nlm.nih.gov/geo/query/acc.cgi?acc=GSE262019).

ACKNOWLEDGMENTS

This work was supported by the Canadian Institutes of Health Research Doctoral Research Award (CIHR/CGS-D; M.R.T), the Raymond Ng Graduate Award and Harry Barberian Research Award from the University of Toronto (M.R.T.), the Krembil Foundation biomedical research grant (A.D.), and the Michael and Sonja Koerner Charitable Foundation (A.D.). This work was supported (in part) by the Intramural Research Program of the National Institute on Deafness and Other Communication Disorders (NIH Intramural Research Funds ZIA DC000088 to M.H. of the Auditory Development and Restoration Program and ZIC DC000086 to R.J.M. of the NIDCD/NIDCR Genomics and Computational Biology Core), National Institutes of Health, United States. We thank Dr. Martín Basch for his helpful discussions, leading to the generation the P1 single-cell RNA sequencing dataset. We also acknowledge the imaging facilities at Sunnybrook Research Institute and The Hospital for Sick Children, Toronto, Canada, for the use of and assistance with confocal microscopy. We thank Dr. Yutaka Amemiya and the Genomics Core Facility at Sunnybrook Research Institute for discussions and data analysis concerning reverse transcription quantitative real-time PCR. We also acknowledge the Ottawa Bioinformatics Core Facility for assisting with conducting bioinformatic analyses. This work utilized the computational resources of the NIH HPC Biowulf cluster (https://hpc.nih.gov).

AUTHOR CONTRIBUTIONS

Conceptualization, M.R.T., M.H., and A.D.; data curation, M.R.T., R.Y., and S.G.; formal analysis, M.R.T., R.Y., S.G., R.J.M., and M.H.; funding acquisition, M.R.T., R.J.M., A.D., and M.H.; investigation, M.R.T., R.T.O., S.G., R.J.M., and M.H.; methodology, M.R.T., R.T.O., S.G., M.H., and A.D.; supervision, A.D.; writing—original draft, M.R.T.; writing—review & editing, M.R.T., R.Y., R.T.O., S.G., R.J.M., M.H., and A.D.

DECLARATION OF INTERESTS

The authors declare no competing interests.

STAR★METHODS

Detailed methods are provided in the online version of this paper and include the following:

- KEY RESOURCES TABLE
- EXPERIMENTAL MODEL AND STUDY PARTICIPANT DETAILS
- METHOD DETAILS
  - Stria vascularis organotypic explant cultures
  - In vitro proliferation assays
  - Wnt inhibition
  - reverse transcription quantitative real-time PCR
  - Tissue cryosection
  - Immunofluorescence
  - RNAscope™
  - Microscopy
  - Cell quantification

- SV sample preparation for scRNA sequencing
- 10× chromium genomics platform
- Single cell RNA-sequencing data preprocessing
- Dimensionality reduction and clustering
- Differential expression analysis
- CellChat analysis
- Trajectory analysis

- QUANTIFICATION AND STATISTICAL ANALYSIS

SUPPLEMENTAL INFORMATION

Supplemental information can be found online at https://doi.org/10.1016/j.isci.2025.111832.

Received: April 5, 2024
Revised: July 31, 2024
Accepted: January 15, 2025
Published: January 17, 2025

REFERENCES

1. Kikuchi, K., and Hilding, D.A. (1966). The development of the stria vascularis in the mouse. Acta Otolaryngol. *62*, 277–291. https://doi.org/10.3109/00016486609119573.
2. Morell, R.J., Olszewski, R., Tona, R., Leitess, S., Wafa, T.T., Taukulis, I., Schultz, J.M., Thomason, E.J., Richards, K., Whitley, B.N., et al. (2020). Noncoding microdeletion in mouse Hgf disrupts neural crest migration into the stria vascularis, reduces the endocochlear potential, and suggests the neuropathology for human nonsyndromic deafness DFNB39. J. Neurosci. *40*, 2976–2992. https://doi.org/10.1523/JNEUROSCI.2278-19.2020.
3. Renauld, J.M., Khan, V., and Basch, M.L. (2022). Intermediate cells of dual embryonic origin follow a basal to apical gradient of ingression into the lateral wall of the cochlea. Front. Cell Dev. Biol. *10*, 867153. https://doi.org/10.3389/fcell.2022.867153.
4. Shibata, S., Miwa, T., Wu, H.-H., Levitt, P., and Ohyama, T. (2016). Hepatocyte growth factor–c-MET signaling mediates the development of nonsensory structures of the mammalian cochlea and hearing. J. Neurosci. *36*, 8200–8209. https://doi.org/10.1523/JNEUROSCI.4410-15.2016.
5. Steel, K.P., and Barkway, C. (1989). Another role for melanocytes: Their importance for normal stria vascularis development in the mammalian inner ear. Development *107*, 453–463. https://doi.org/10.1242/dev.107.3.453.
6. Udagawa, T., Takahashi, E., Tatsumi, N., Mutai, H., Saijo, H., Kondo, Y., Atkinson, P.J., Matsunaga, T., Yoshikawa, M., Kojima, H., et al. (2024). Loss of Pax3 causes reduction of melanocytes in the developing mouse cochlea. Sci. Rep. *14*, 2210. https://doi.org/10.1038/s41598-024-52629-9.
7. Shi, X. (2011). Physiopathology of the cochlear microcirculation. Hear. Res. *282*, 10–24. https://doi.org/10.1016/j.heares.2011.08.006.
8. Carraro, M., and Harrison, R.V. (2016). Degeneration of stria vascularis in age-related hearing loss; a corrosion cast study in a mouse model. Acta Otolaryngol. *136*, 385–390. https://doi.org/10.3109/00016489.2015.1123291.
9. Liu, W., Schrott-Fischer, A., Glueckert, R., Benav, H., and Rask-Andersen, H. (2017). The human "cochlear battery"—claudin-11 barrier and ion transport proteins in the lateral wall of the cochlea. Front. Mol. Neurosci. *10*, 239. https://doi.org/10.3389/fnmol.2017.00239.
10. Locher, H., de Groot, J.C.M.J., van Iperen, L., Huisman, M.A., Frijns, J.H.M., and Chuva de Sousa Lopes, S.M. (2015). Development of the stria vascularis and potassium regulation in the human fetal cochlea: Insights into hereditary sensorineural hearing loss. Dev. Neurobiol. *75*, 1219–1240. https://doi.org/10.1002/dneu.22279.
11. Trowe, M.-O., Maier, H., Petry, M., Schweizer, M., Schuster-Gossler, K., and Kispert, A. (2011). Impaired stria vascularis integrity upon loss of E-cadherin in basal cells. Dev. Biol. *359*, 95–107. https://doi.org/10.1016/j.ydbio.2011.08.030.
12. Bryant, D., Pauzuolyte, V., Ingham, N.J., Patel, A., Pagarkar, W., Anderson, L.A., Smith, K.E., Moulding, D.A., Leong, Y.C., Jafree, D.J., et al. (2022). The timing of auditory sensory deficits in Norrie disease has implications for therapeutic intervention. JCI Insight *7*, e148586. https://doi.org/10.1172/jci.insight.148586.
13. Breglio, A.M., Rusheen, A.E., Shide, E.D., Fernandez, K.A., Spielbauer, K.K., McLachlin, K.M., Hall, M.D., Amable, L., and Cunningham, L.L. (2017). Cisplatin is retained in the cochlea indefinitely following chemotherapy. Nat. Commun. *8*, 1654. https://doi.org/10.1038/s41467-017-01837-1.
14. Lang, H., Noble, K.V., Barth, J.L., Rumschlag, J.A., Jenkins, T.R., Storm, S.L., Eckert, M.A., Dubno, J.R., and Schulte, B.A. (2023). The stria vascularis in mice and humans is an early site of age-related cochlear degeneration, macrophage dysfunction, and inflammation. J. Neurosci. *43*, 5057–5075. https://doi.org/10.1523/JNEUROSCI.2234-22.2023.
15. Rehm, H.L., Zhang, D.-S., Brown, M.C., Burgess, B., Halpin, C., Berger, W., Morton, C.C., Corey, D.P., and Chen, Z.-Y. (2002). Vascular Defects and Sensorineural Deafness in a Mouse Model of Norrie Disease. J. Neurosci. *22*, 4286–4292. https://doi.org/10.1523/JNEUROSCI.22-11-04286.2002.
16. Thulasiram, M.R., Ogier, J.M., and Dabdoub, A. (2022). Hearing function, degeneration, and disease: Spotlight on the stria vascularis. Front. Cell Dev. Biol. *10*, 841708. https://doi.org/10.3389/fcell.2022.841708.
17. Wan, H., Chen, H., Liu, J., Yang, B., Zhang, Y., Bai, Y., Chen, X., Wang, J., Liu, T., Zhang, Y., and Hua, Q. (2024). PARP1 inhibition prevents oxidative stress in age-related hearing loss via PAR-Ca2+-AIF axis in cochlear strial marginal cells. Free Radic. Biol. Med. *220*, 222–235. https://doi.org/10.1016/j.freeradbiomed.2024.05.020.
18. Zhang, N., Cai, J., Xu, L., Wang, H., and Liu, W. (2020). Cisplatin-induced stria vascularis damage is associated with inflammation and fibrosis. Neural Plast. *2020*, 8851525. https://doi.org/10.1155/2020/8851525.
19. Haque, K.D., Pandey, A.K., Kelley, M.W., and Puligilla, C. (2015). Culture of embryonic mouse cochlear explants and gene transfer by electroporation. J. Vis. Exp. *95*, 52260. https://doi.org/10.3791/52260.
20. Kelley, M.W., Talreja, D.R., and Corwin, J.T. (1995). Replacement of hair cells after laser microbeam irradiation in cultured organs of Corti from embryonic and neonatal mice. J. Neurosci. *15*, 3013–3026. https://doi.org/10.1523/JNEUROSCI.15-04-03013.1995.
21. Warchol, M.E., Lambert, P.R., Goldstein, B.J., Forge, A., and Corwin, J.T. (1993). Regenerative proliferation in inner ear sensory epithelia from adult guinea pigs and humans. Science *259*, 1619–1622. https://doi.org/10.1126/science.8456285.
22. Neng, L., Zhang, F., Kachelmeier, A., and Shi, X. (2013). Endothelial cell, pericyte, and perivascular resident macrophage-type melanocyte interactions regulate cochlear intrastrial fluid–blood barrier permeability. J. Assoc. Res. Otolaryngol. *14*, 175–185. https://doi.org/10.1007/s10162-012-0365-9.
23. Wang, W., Flores, M.C.P., Sihn, C.-R., Kim, H.J., Zhang, Y., Doyle, K.J., Chiamvimonvat, N., Zhang, X.-D., and Yamoah, E.N. (2015). Identification of a key residue in Kv7.1 potassium channel essential for sensing external potassium ions. J. Gen. Physiol. *145*, 201–212. https://doi.org/10.1085/jgp.201411280.
24. Yi, Y., Wang, X.-R., Chen, H.-T., Huang, W.-Y., Feng, L.-X., Fang, S.-B., and Xiong, G.-X. (2023). Development of a serum-free culture method for endothelial cells of the stria vascularis and their pro-inflammatory secretome changes induced by oxidative stress. Clin. Exp. Otorhinolaryngol. *16*, 37–48. https://doi.org/10.21053/ceo.2022.01172.
25. Davis, R.L., Lopez, C.A., and Mou, K. (1995). Expression of osteopontin in the inner ear. Ann. N. Y. Acad. Sci. *760*, 279–295. https://doi.org/10.1111/j.1749-6632.1995.tb44638.x.

26. Mou, K., Adamson, C.L., and Davis, R.L. (1997). Stria vascularis morphogenesis in vitro. Hear. Res. *103*, 47–62. https://doi.org/10.1016/S0378-5955(96)00163-3.

27. Zhang, J., Hou, Z., Wang, X., Jiang, H., Neng, L., Zhang, Y., Yu, Q., Burwood, G., Song, J., Auer, M., et al. (2021). VEGFA165 gene therapy ameliorates blood-labyrinth barrier breakdown and hearing loss. JCI Insight *6*, e143285. https://doi.org/10.1172/jci.insight.143285.

28. Gu, S., Olszewski, R., Taukulis, I., Wei, Z., Martin, D., Morell, R.J., and Hoa, M. (2020). Characterization of rare spindle and root cell transcriptional profiles in the stria vascularis of the adult mouse cochlea. Sci. Rep. *10*, 18100. https://doi.org/10.1038/s41598-020-75238-8.

29. Jean, P., Tai, F.W.J., Singh-Estivalet, A., Lelli, A., Scandola, C., Megharba, S., Schmutz, S., Roux, S., Mechaussier, S., Sudresm, M., et al. (2023). Single- cell transcriptomic profiling of the mouse cochlea: An atlas for targeted therapies. Proc. Natl. Acad. Sci. USA *120*, e2221744120. https://doi.org/10.1073/pnas.2221744120.

30. Korrapati, S., Taukulis, I., Olszewski, R., Pyle, M., Gu, S., Singh, R., Griffiths, C., Martin, D., Boger, E., Morell, R.J., and Hoa, M. (2019). Single cell and single nucleus RNA-seq reveal cellular heterogeneity and homeostatic regulatory networks in adult mouse stria vascularis. Front. Mol. Neurosci. *12*, 316. https://doi.org/10.3389/fnmol.2019.00316.

31. Milon, B., Shulman, E.D., So, K.S., Cederroth, C.R., Lipford, E.L., Sperber, M., Sellon, J.B., Sarlus, H., Pregernig, G., Shuster, B., et al. (2021). A cell-type-specific atlas of the inner ear transcriptional response to acoustic trauma. Cell Rep. *36*. https://doi.org/10.1016/j.celrep.2021.109758.

32. Taukulis, I.A., Olszewski, R.T., Korrapati, S., Fernandez, K.A., Boger, E.T., Fitzgerald, T.S., Morell, R.J., Cunningham, L.L., and Hoa, M. (2021). Single-cell RNA-seq of cisplatin-treated adult stria vascularis identifies cell type-specific regulatory networks and novel therapeutic gene targets. Front. Mol. Neurosci. *14*, 718241. https://doi.org/10.3389/fnmol.2021.718241.

33. Miller, I., Min, M., Yang, C., Tian, C., Gookin, S., Carter, D., and Spencer, S.L. (2018). Ki67 is a graded rather than a binary marker of proliferation versus quiescence. Cell Rep. *24*, 1105–1112.e5. https://doi.org/10.1016/j.celrep.2018.06.110.

34. Sobecki, M., Mrouj, K., Camasses, A., Parisis, N., Nicolas, E., Llères, D., Gerbe, F., Prieto, S., Krasinska, L., David, A., et al. (2016). The cell proliferation antigen Ki-67 organises heterochromatin. Elife *5*, e13722. https://doi.org/10.7554/eLife.13722.001.

35. Steinhart, Z., and Angers, S. (2018). Wnt signaling in development and tissue homeostasis. Development *145*, dev146589. https://doi.org/10.1242/dev.146589.

36. Jacques, B.E., Puligilla, C., Weichert, R.M., Ferrer-Vaquer, A., Hadjantonakis, A.K., Kelley, M.W., and Dabdoub, A. (2012). A dual function for canonical Wnt/β-catenin signaling in the developing mammalian cochlea. Development *139*, 4395–4404. https://doi.org/10.1242/dev.080358.

37. Samarajeewa, A., Lenz, D.R., Xie, L., Chiang, H., Kirchner, R., Mulvaney, J.F., Edge, A.S.B., and Dabdoub, A. (2018). Transcriptional response to Wnt activation regulates the regenerative capacity of the mammalian cochlea. Development *145*, dev166579. https://doi.org/10.1242/dev.166579.

38. Geng, R., Noda, T., Mulvaney, J.F., Lin, V.Y.W., Edge, A.S.B., and Dabdoub, A. (2016). Comprehensive expression of Wnt signaling pathway genes during development and maturation of the mouse cochlea. PLoS One *11*, e0148339. https://doi.org/10.1371/journal.pone.0148339.

39. Samarajeewa, A., Jacques, B.E., and Dabdoub, A. (2019). Therapeutic potential of Wnt and Notch signaling and epigenetic regulation in mammalian sensory hair cell regeneration. Mol. Ther. *27*, 904–911. https://doi.org/10.1016/j.ymthe.2019.03.017.

40. Furness, D.N. (2019). Forgotten fibrocytes: A neglected, supporting cell type of the cochlea with the potential to be an alternative therapeutic target in hearing loss. Front. Cell. Neurosci. *13*, 532. https://doi.org/10.3389/fncel.2019.00532.

41. Peeleman, N., Verdoodt, D., Ponsaerts, P., and Van Rompaey, V. (2020). On the role of fibrocytes and the extracellular matrix in the physiology and pathophysiology of the spiral ligament. Front. Neurol. *11*, 580639. https://doi.org/10.3389/fneur.2020.580639.

42. Kamiya, K., Fujinami, Y., Hoya, N., Okamoto, Y., Kouike, H., Komatsuzaki, R., Kusano, R., Nakagawa, S., Satoh, H., Fujii, M., and Matsunaga, T. (2007). Mesenchymal stem cell transplantation accelerates hearing recovery through the repair of injured cochlear fibrocytes. Am. J. Pathol. *171*, 214–226. https://doi.org/10.2353/ajpath.2007.060948.

43. Stevens, S.M., Xing, Y., Hensley, C.T., Zhu, J., Dubno, J.R., and Lang, H. (2014). Heptanol application to the mouse round window: A model for studying cochlear lateral wall regeneration. Otolaryngol. Head Neck Surg. *150*, 659–665. https://doi.org/10.1177/0194599813518876.

44. Chen, J., Chen, P., He, B., Gong, T., Li, Y., Zhang, J., Lv, J., Mammano, F., Hou, S., and Yang, J. (2021). Connexin30-deficiency causes mild hearing loss with the reduction of endocochlear potential and ATP release. Front. Cell. Neurosci. *15*, 819194–819212. https://doi.org/10.3389/fncel.2021.819194.

45. Mei, L., Chen, J., Zong, L., Zhu, Y., Liang, C., Jones, R.O., and Zhao, H.-B. (2017). A deafness mechanism of digenic Cx26 (GJB2) and Cx30 (GJB6) mutations: Reduction of endocochlear potential by impairment of heterogeneous gap junctional function in the cochlear lateral wall. Neurobiol. Dis. *108*, 195–203. https://doi.org/10.1016/j.nbd.2017.08.002.

46. Tsuprun, V., and Santi, P. (1999). Ultrastructure and immunohistochemical identification of the extracellular matrix of the chinchilla cochlea. Hear. Res. *129*, 35–49. https://doi.org/10.1016/s0378-5955(98)00219-6.

47. Neng, L., Zhang, J., Yang, J., Zhang, F., Lopez, I.A., Dong, M., and Shi, X. (2015). Structural changes in thestrial blood–labyrinth barrier of aged C57BL/6 mice. Cell Tissue Res. *361*, 685–696. https://doi.org/10.1007/s00441-015-2147-2.

48. Zhang, W., Dai, M., Fridberger, A., Hassan, A., DeGagne, J., Neng, L., Zhang, F., He, W., Ren, T., Trune, D., et al. (2012). Perivascular-resident macrophage-like melanocytes in the inner ear are essential for the integrity of the intrastrial fluid-blood barrier. Proc. Natl. Acad. Sci. USA *109*, 10388–10393. https://doi.org/10.1073/pnas.1205210109.

49. Adameyko, I., Lallemend, F., Aquino, J.B., Pereira, J.A., Topilko, P., Müller, T., Fritz, N., Beljajeva, A., Mochii, M., Liste, I., et al. (2009). Schwann cell precursors from nerve innervation are a cellular origin of melanocytes in skin. Cell *139*, 366–379. https://doi.org/10.1016/j.cell.2009.07.049.

50. Aoki, H., Yamada, Y., Hara, A., and Kunisada, T. (2009). Two distinct types of mouse melanocyte: Differential signaling requirement for the maintenance of non-cutaneous and dermal versus epidermal melanocytes. Development *136*, 2511–2521. https://doi.org/10.1242/dev.037168.

51. Bonnamour, G., Soret, R., and Pilon, N. (2021). Dhh-expressing Schwann cell precursors contribute to skin and cochlear melanocytes, but not to vestibular melanocytes. Pigment Cell Melanoma Res. *34*, 648–654. https://doi.org/10.1111/pcmr.12938.

52. Li, H.-L., Qu, Y.-J., Lu, Y.C., Bondarenko, V.E., Wang, S., Skerrett, I.M., and Morales, M.J. (2006). Dpp10 is an inactivation modulatory protein of Kv4.3 and Kv1.4. Am. J. Physiol. Cell Physiol. *291*, C966–C976. https://doi.org/10.1152/ajpcell.00571.2005.

53. Neef, J., Gehrt, A., Bulankina, A.V., Meyer, A.C., Riedel, D., Gregg, R.G., Strenzke, N., and Moser, T. (2009). The Ca2+ channel subunit β2 regulates Ca2+ channel abundance and function in inner hair cells and is required for hearing. J. Neurosci. *29*, 10730–10740. https://doi.org/10.1523/JNEUROSCI.1577-09.2009.

54. Miwa, T., Minoda, R., Ishikawa, Y., Kajii, T., Orita, Y., and Ohyama, T. (2019). Role of Dach1 revealed using a novel inner ear-specific Dach1-knockdown mouse model. Biol. Open *8*, bio043612. https://doi.org/10.1242/bio.043612.

55. Nabec, A.L., Blotas, C., Briset, A., Collobert, M., Férec, C., and Moisan, S. (2022). 3D chromatin organization involving MEIS1 factor in the cis-regulatory landscape of GJB2. Int. J. Mol. Sci. *23*, 1–13. https://doi.org/10.3390/ijms23136964.

56. Cosgrove, D., Samuelson, G., Meehan, D.T., Miller, C., McGee, J., Walsh, E.J., and Siegel, M. (1998). Ultrastructural, physiological, and molecular defects in the inner ear of a gene-knockout mouse model for autosomal Alport syndrome. Hear. Res. *121*, 84–98. https://doi.org/10.1016/S0378-5955(98)00069-0.

57. Dufek, B., Meehan, D.T., Delimont, D., Wilhelm, K., Samuelson, G., Coenen, R., Madison, J., Doyle, E., Smyth, B., Phillips, G., et al. (2020). RNA-seq analysis of gene expression profiles in isolated stria vascularis from wild-type and Alport mice reveals key pathways underling Alport strial pathogenesis. PLoS One *15*, e0237907. https://doi.org/10.1371/journal.pone.0237907.

58. Meyer Zum Gottesberge, A.M., Gross, O., Becker-Lendzian, U., Massing, T., and Vogel, W.F. (2008). Inner ear defects and hearing loss in mice lacking the collagen receptor DDR1. Lab. Invest. *88*, 27–37. https://doi.org/10.1038/labinvest.3700692.

59. Gow, A., Davies, C., Southwood, C.M., Frolenkov, G., Chrustowski, M., Ng, L., Yamauchi, D., Marcus, D.C., and Kachar, B. (2004). Deafness in claudin 11-null mice reveals the critical contribution of basal cell tight junctions to stria vascularis function. J. Neurosci. *24*, 7051–7062. https://doi.org/10.1523/JNEUROSCI.1640-04.2004.

60. Kitajiri, S.-I., Miyamoto, T., Mineharu, A., Sonoda, N., Furuse, K., Hata, M., Sasaki, H., Mori, Y., Kubota, T., Ito, J., et al. (2004). Compartmentalization established by claudin-11-based tight junctions in stria vascularis is required for hearing through generation of endocochlear potential. J. Cell Sci. *117*, 5087–5096. https://doi.org/10.1242/jcs.01393.

61. Papadimitriou, E., Mourkogianni, E., Ntenekou, D., Christopoulou, M., Koutsioumpa, M., and Lamprou, M. (2022). On the role of pleiotrophin and its receptors in development and angiogenesis. Int. J. Dev. Biol. *66*, 115–124. https://doi.org/10.1387/ijdb.210122ep.

62. Sone, M., Muramatsu, H., Muramatsu, T., and Nakashima, T. (2011). Morphological observation of the stria vascularis in midkine and pleiotrophin knockout mice. Auris Nasus Larynx *38*, 41–45. https://doi.org/10.1016/j.anl.2010.05.005.

63. Defourny, J. (2019). Eph/ephrin signalling in the development and function of the mammalian cochlea. Dev. Biol. *449*, 35–40. https://doi.org/10.1016/j.ydbio.2019.02.004.

64. Yim, A., Smith, C., and Brown, A.M. (2022). Osteopontin/secreted phosphoprotein-1 harnesses glial-immune-and neuronal cell ligand-receptor interactions to sense and regulate acute and chronic neuroinflammation. Immunol. Rev. *311*, 224–233. https://doi.org/10.1111/imr.13081.

65. McInturff, S., Burns, J.C., and Kelley, M.W. (2018). Characterization of spatial and temporal development of Type I and Type II hair cells in the mouse utricle using new cell-type-specific markers. Biol. Open *7*, bio038083. https://doi.org/10.1242/bio.038083.

66. Meyer, R.C., Giddens, M.M., Coleman, B.M., and Hall, R.A. (2014). The protective role of prosaposin and its receptors in the nervous system. Brain Res. *1585*, 1–12. https://doi.org/10.1016/j.brainres.2014.08.022.

67. Akil, O., Chang, J., Hiel, H., Kong, J.-H., Yi, E., Glowatzki, E., and Lustig, L.R. (2006). Progressive deafness and altered cochlear innervation in knock-out mice lacking prosaposin. J. Neurosci. *26*, 13076–13088. https://doi.org/10.1523/JNEUROSCI.3746-06.2006.

68. Terashita, T., Saito, S., Miyawaki, K., Hyodo, M., Kobayashi, N., Shimokawa, T., Saito, K., Matsuda, S., and Gyo, K. (2007). Localization of prosaposin in rat cochlea. Neurosci. Res. *57*, 372–378. https://doi.org/10.1016/j.neures.2006.11.006.

69. Díaz-Coránguez, M., Lin, C.-M., Liebner, S., and Antonetti, D.A. (2020). Norrin restores blood-retinal barrier properties after vascular endothelial growth factor-induced permeability. J. Biol. Chem. *12*, 1–31. https://doi.org/10.1074/jbc.RA119.011273.

70. Lopez, C.A., Olson, E.S., Adams, J.C., Mou, K., Denhardt, D.T., and Davis, R.L. (1995). Osteopontin expression detected in adult cochleae and inner ear fluids. Hear. Res. *85*, 210–222. https://doi.org/10.1016/0378-5955(95)00046-7.

71. Du, Y.-Y., Zhao, Y.-X., Liu, Y.-P., Liu, W., Wang, M.-M., and Yuan, C.-M. (2015). Regulatory Tweak/Fn14 signaling pathway as a potent target for controlling bone loss. Biomed. Pharmacother. *70*, 170–173. https://doi.org/10.1016/j.biopha.2015.01.005.

72. Ratajczak, W., Atkinson, S.D., and Kelly, C. (2022). The TWEAK/Fn14/CD163 axis—implications for metabolic disease. Rev. Endocr. Metab. Disord. *23*, 449–462. https://doi.org/10.1007/s11154-021-09688-4.

73. Winkles, J.A. (2008). The TWEAK-Fn14 cytokine-receptor axis: Discovery, biology and therapeutic targeting. Nat. Rev. Drug Discov. *7*, 411–425. https://doi.org/10.1038/nrd2488.

74. Frejo, L., Requena, T., Okawa, S., Gallego-Martinez, A., Martinez-Bueno, M., Aran, I., Batuecas-Caletrio, A., Benitez-Rosario, J., Espinosa-Sanchez, J.M., Fraile-Rodrigo, J.J., et al. (2017). Regulation of Fn14 receptor and NF-κB underlies inflammation in Meniere's disease. Front. Immunol. *8*, 1739. https://doi.org/10.3389/fimmu.2017.01739.

75. Kaucka, M., Szarowska, B., Kavkova, M., Kastriti, M.E., Kameneva, P., Schmidt, I., Peskova, L., Joven Araus, A., Simon, A., Kaiser, J., and Adameyko, I. (2021). Nerve-associated Schwann cell precursors contribute extracutaneous melanocytes to the heart, inner ear, supraorbital locations and brain meninges. Cell. Mol. Life Sci. *78*, 6033–6049. https://doi.org/10.1007/s00018-021-03885-9.

76. Renauld, J.M., Davis, W., Cai, T., Cabrera, C., and Basch, M.L. (2021). Transcriptomic analysis and ednrb expression in cochlear intermediate cells reveal developmental differences between inner ear and skin melanocytes. Pigment Cell Melanoma Res. *34*, 585–597. https://doi.org/10.1111/pcmr.12961.

77. Ritter, K.E., and Martin, D.M. (2019). Neural crest contributions to the ear: Implications for congenital hearing disorders. Hear. Res. *376*, 22–32. https://doi.org/10.1016/j.heares.2018.11.005.

78. Yoshimura, N., Motohashi, T., Aoki, H., Tezuka, K.I., Watanabe, N., Wakaoka, T., Era, T., and Kunisada, T. (2013). Dual origin of melanocytes defined by Sox1 expression and their region-specific distribution in mammalian skin. Dev. Growth Differ. *55*, 270–281. https://doi.org/10.1111/dgd.12034.

79. Yu, W., Zong, S., Du, P., Zhou, P., Li, H., Wang, E., and Xiao, H. (2021). Role of the stria vascularis in the pathogenesis of sensorineural hearing loss: A narrative review. Front. Neurosci. *15*, 774585. https://doi.org/10.3389/fnins.2021.774585.

80. Wang, Y., Rattner, A., Zhou, Y., Williams, J., Smallwood, P.M., and Nathans, J. (2012). Norrin/Frizzled4 signaling in retinal vascular development and blood brain barrier plasticity. Cell *151*, 1332–1344. https://doi.org/10.1016/j.cell.2012.10.042.

81. Xu, Q., Wang, Y., Dabdoub, A., Smallwood, P.M., Williams, J., Woods, C., Kelley, M.W., Jiang, L., Tasman, W., Zhang, K., and Nathans, J. (2004). Vascular development in the retina and inner ear: Control by Norrin and Frizzled-4, a high-affinity ligand-receptor pair. Cell *116*, 883–895. https://doi.org/10.1016/S0092-8674(04)00216-8.

82. Pauzuolyte, V., Patel, A., Wawrzynski, J.R., Ingham, N.J., Leong, Y.C., Karda, R., Bitner-Glindzicz, M., Berger, W., Waddington, S.N., Steel, K.P., and Sowden, J.C. (2023). Systemic gene therapy rescues retinal dysfunction and hearing loss in a model of Norrie disease. EMBO Mol. Med. *15*, 173933–e17424. https://doi.org/10.15252/emmm.202317393.

83. Jin, S., Guerrero-Juarez, C.F., Zhang, L., Chang, I., Ramos, R., Kuan, C.-H., Myung, P., Plikus, M.V., and Nie, Q. (2021). Inference and analysis of cell-cell communication using CellChat. Nat. Commun. *12*, 1088. https://doi.org/10.1038/s41467-021-21246-9.

84. Street, K., Risso, D., Fletcher, R.B., Das, D., Ngai, J., Yosef, N., Purdom, E., and Dudoit, S. (2018). Slingshot: Cell lineage and pseudotime inference for single-cell transcriptomics. BMC Genom. *19*, 1–16. https://doi.org/10.1186/s12864-018-4772-0.

85. Shimoyama, Y. (2022). pyCirclize: Circular visualization in Python [Computer software]. https://github.com/moshi4/pyCirclize.

86. Stuart, T., Butler, A., Hoffman, P., Hafemeister, C., Papalexi, E., Mauck, W.M., 3rd, Hao, Y., Stoeckius, M., Smibert, P., and Satija, R. (2019). Comprehensive integration of single-cell data. Cell *177*, 1888–1902.e21. https://doi.org/10.1016/j.cell.2019.05.031.

87. Hao, Y., Hao, S., Andersen-Nissen, E., Mauck, W.M., 3rd, Zheng, S., Butler, A., Lee, M.J., Wilk, A.J., Darby, C., Zager, M., et al. (2021). Integrated analysis of multimodal single-cell data. Cell *184*, 3573–3587.e29. https://doi.org/10.1016/j.cell.2021.04.048.

88. Choudhary, S., and Satija, R. (2022). Comparison and evaluation of statistical error models for scRNA-seq. Genome Biol. *23*, 27. https://doi.org/10.1186/s13059-021-02584-9.

89. Waltman, L., and van Eck, N.J. (2013). A smart local moving algorithm for large-scale modularity-based community detection. Eur. Phys. J. B *86*, 471. https://doi.org/10.1140/epjb/e2013-40829-0.

90. Cao, J., Spielmann, M., Qiu, X., Huang, X., Ibrahim, D.M., Hill, A.J., Zhang, F., Mundlos, S., Christiansen, L., Steemers, F.J., et al. (2019). The single-cell transcriptional landscape of mammalian organogenesis. Nature *566*, 496–502. https://doi.org/10.1038/s41586-019-0969-x.

STAR★METHODS

KEY RESOURCES TABLE

REAGENT or RESOURCE	SOURCE	IDENTIFIER
Antibodies		
Mouse anti-BrdU	BD Biosciences	Cat #555627; RRID: AB_395993
Rabbit anti-Ki67	Abcam	Cat# Ab15580; RRID: AB_443209
Rabbit anti-Cldn11	Santa Cruz	Cat# sc-25711; RRID: 639330
Guinea pig anti-Kcnq1	Alomone Labs	APC-022-GP; RRID: AB_2827303
Chemicals, peptides, and recombinant proteins		
Corning™ Matrigel™ Matrix	Fisher Scientific	Cat# CB-40234
Bromodeoxyuridine (BrdU)	BD Pharmingen™	Cat# 550891
β-catenin/Tcf inhibitor FH535	EMD Millipore	CAS 108409-83-2
Osteosoft®	Millipore Sigma	Cat# 1017281000
Tissue Tek® O.C.T. Compound	Sakura	Cat# 4583
Griffonia (Bandeiraea) Simplicifolia Lectin I (GSL I, BSL I), Fluorescein	Vector Laboratories	FL-1101-2
Griffonia (Bandeiraea) Simplicifolia Lectin I (GSL I, BSL I), Rhodamine	Vector Laboratories	RL-1102-2
DAPI	Sigma-Aldrich	D9542
TSA vivid dyes 570	Advanced Cell Diagnostics	Cat# 323272
TSA vivid dye 650	Advanced Cell Diagnostics	Cat# 323273
Trypsin	Worthington Biochemical Corporation	Cat# LS003708
Accutase®	Sigma-Aldrich	Cat# A6964-100ML
Critical commercial assays		
RNAqueous™-Micro Total RNA Isolation Kit	Invitrogen™	Cat# AM1931
High-Capacity RNA-to-cDNA™	Applied Biosystems™	Cat# 4387406
TaqMan™ Fast Advanced Master Mix	Applied Biosystems™	Cat# 4444556
RNAscope™ Mutiplex Fluroescent Assay V2	Advanced Cell Diagnostics	Cat# 323100
Deposited data		
Raw and analyzed data	This paper	GEO Series accession ID: GSE262019, https://www.ncbi.nlm.nih.gov/geo/query/acc.cgi?acc=GSE262019
Experimental models: Organisms/strains		
Mouse: CD-1	Charles River Laboratory	Strain code: 022
Mouse: CBA/J	The Jackson Laboratory	JAX: 000656
Oligonucleotides		
GAPDH Mm99999915_g1	ThermoFisher Scientific	Cat# 4331182
mKi67 Mm01278617_m1	Thermo Fisher Scientific	Cat# 4331182
Kcnq1 Mm00434640_m1	Thermo Fisher Scientific	Cat# 4331182
Kcnj10 Mm00445028_m1	Thermo Fisher Scientific	Cat# 4331182
Cldn11 Mm00500915_m1	Thermo Fisher Scientific	Cat# 4331182
Mm Trpm1-C1 (17364)	Advanced Cell Diagnostics	Cat# 858561
Mm Col5a3-C1 (53867)	Advanced Cell Diagnostics	Cat# 577221
Mm Kcnj10-C3 (16513)	Advanced Cell Diagnostics	Cat# 458831-C3
Mm Plp1-C4 (18823)	Advanced Cell Diagnostics	Cat# 428181-C4
Mm Ldha-C2	Advanced Cell Diagnostics	N/A custom probe

(*Continued on next page*)

Continued

REAGENT or RESOURCE	SOURCE	IDENTIFIER
Mm Dpp10-C3	Advanced Cell Diagnostics	N/A custom probe
Software and algorithms		
R (v4.3.0–4.4.2)	https://cran.r-project.org/	https://cran.r-project.org/
CellChat (v1.5.0)	Jin et al.[83]	https://github.com/sqjin/CellChat
Slingshot (v1.6.0)	Street et al.[84]	https://github.com/kstreet13/slingshot
pyCirclize	Shimoyama[85]	https://github.com/moshi4/pyCirclize
Seurat (v3)	Stuart et al.[86]	https://github.com/satijalab/seurat/releases/tag/v3.0.0
Seurat (v4)	Hao et al.[87]	https://github.com/satijalab/seurat

EXPERIMENTAL MODEL AND STUDY PARTICIPANT DETAILS

Care and euthanasia of male and female CD-1 mice (Charles River Laboratory) used in this study was approved by the Institutional Animal Care and Use Committee (ACC) regulations at Sunnybrook Research Institute in Toronto, Canada (ACC protocol no. 23515). Primary tissue for culture was collected from postnatal day 1 (P1) up to P36 CD-1 mice. CBA/J mice were purchased from JAX (Stock No. 000656) and P1 and P30 mice were used for single cell RNA-sequencing experiments. The animal study was reviewed and approved by Animal Care and Use Committee of the National Institute of Neurological Diseases and Stroke and the National Institute on Deafness and Other Communication Disorders, National Institutes of Health.

METHOD DETAILS

Stria vascularis organotypic explant cultures

Inner ears were dissected from neonatal and functionally mature mice in ice-cold HBSS with 1% HEPES. In neonatal pups, the cartilaginous membrane over the cochlea was carefully removed, and in P30 mice, the bone was carefully chipped off, to expose the cochlear tissue. The cochlear duct was removed from the modiolus, and the lateral wall was removed from the sensory epithelium. Then, the SV was gently teased away from the spiral ligament to isolate only the three cell layers of the SV. After verifying the isolation of the SV cell types through immunohistochemistry and transcriptomics, SV were cultured in 2.5% FBS media in a 10 mm glass bottom dish coated with Matrigel for a total of 72 h (h) at 37°C. All experiments were stopped after 72 h, then explants were rinsed with PBS and fixed with 4% paraformaldehyde. Culture conditions were modified from a previously established technique for cochlear explants.[37]

In vitro proliferation assays

The thymidine analog 5-bromo-2′-deoxyuridine (BrdU; BD Biosciences 550891) was used to assess cell proliferation *in vitro*. SV from postnatal day (P) 0–1 mice were exposed to 3.5 μg/mL BrdU for the following durations: 1.5 h (n = 11), 5 h (n = 10), 9 h (n = 10), 24 h (n = 13), 48 h (n = 12), and 72 h (n = 14). Proliferation was also assessed throughout postnatal age, at P0-1 (n = 10), P7-8 (n = 12), and P30-35 (n = 6).

Wnt inhibition

SV were cultured in the presence of the β-Catenin/Tcf Inhibitor, FH535, at the following concentrations: 1 μM (n = 9), 2.5 μM (n = 10), 5 μM (n = 10), or 10 μM (n = 9); EMD Millipore 219330). DMSO was administered as the vehicle control (n = 9). All explants were cultured with 3.5 μg/mL BrdU for 72 h.

reverse transcription quantitative real-time PCR

reverse transcription quantitative real-time PCR experiments were performed to compare *mKi67* gene expression between neonatal and adult SV, and to compare *mKi67*, *Kcnq1*, *Kcnj10*, and *Cldn11* gene expression between neonatal SV before and after 72h in culture. Eight SV were pooled per sample, and experiments were performed using three biological replicates. RNA was extracted using the RNAqueous-Micro Total RNA Isolation Kit (Invitrogen AM1931), and cDNA was transcribed using the High-Capacity RNA-to-cDNA Kit (Applied Biosystems 4387406) according to manufacturer's instructions. reverse transcription quantitative real-time PCR was performed using the TaqMan Fast Advanced Master Mix (Applied Biosystems 4444556) and run on the Applied Biosystems QuantStudio 5. All probes were tested in triplicate. The TaqMan probes used for reverse transcription quantitative real-time PCR gene expression assays were GAPDH (Mm99999915_g1) mKi67 (Mm01278617_m1), Kcnq1 (Mm00434640_m1) Kcnj10 (Mm00445028_m1), and Cldn11 (Mm00500915_m1).

Tissue cryosection

Inner ears were dissected from P0-1 or P30-35 mice and immediately fixed in 4% paraformaldehyde overnight at 4°C. P30-P35 mouse temporal bones were decalcified in Osteosoft (Millipore Sigma 1017281000) for 24–48 h at 37°C. Temporal bones were cryoprotected in 10%, 20% and 30% sucrose steps before being embedded in Tissue Tek O.C.T. Compound (Sakura 4583). Tissues were sectioned at 10 μm thickness on Superfrost Plus Microscope Slides (Fisher Scientific 12-550-15).

Immunofluorescence

Cryosections were permeabilized with 0.5% Triton X- in PBS and quenched with 0.3 M Glycine in 0.5% Triton X- in PBS. Antigen retrieval was performed prior to staining for BrdU using 1 N HCl for 30 min at room temperature. Sections were then blocked in 10% Donkey Serum for 1 h at room temperature. The following primary antibodies were used: Purified mouse anti-BrdU (1:250; BD Biosciences 555627), rabbit anti-Ki67 (1:500, Abcam ab15580), rabbit anti-Cldn11 (1:250; Santa Cruz sc-25711), rabbit anti-Kir4.1 (1:250; Alomone Labs APC-035), and guinea pig anti-Kcnq1 (1:250; Alomone Labs APC-022-GP). Griffonia (Bandeiraea) Simplicifolia Lectin I (GSL I, BSL I), Fluorescein (1:250; Vector Laboratories FL-1101-2), or Rhodamine (Vector Laboratories RL-1102-2) was used to stain blood vessels. DAPI was used as a counterstain for nuclei (1:1000, Sigma-Aldrich D9542).

RNAscope™

In situ hybridization was performed using RNAscope™ Mutiplex Fluorescent Assay V2 according to manufacturer's instructions (Advanced Cell Diagnostics, Cat. No. 323100). Cryosections were obtained as previously mentioned, serially collecting three sections on each slide. Experiments were performed using three biological replicates and two slides per replicate per probe. The following probes were used: Mm Trpm1-C1 (85854), Mm Col5a3-C1 (577221), Mm Kcnj10-C3 (458831-C3), Mm Plp1-C4 (428181). Customized probes included Mm Ldha-C2 and Mm Dpp10-C3. TSA vivid dyes 570 (323272) and 650 (323273) were used. Slides were mounted using Prolong Gold Antifade Mountant (Fisher Scientific, P36930).

Microscopy

Immunofluorescent images were acquired using a Nikon A1R Laser Scanning Confocal Microscope or a Nikon Eclipse Ti. Z-projections covering the depth of the explant or section were captured and converted into a maximum intensity projection. Large image acquisition was also performed with optimal path stitching and 15% overlap. For explant experiments, signal gain was determined using the control sample and then applied to the treated sample and were kept consistent between experimental repeats. RNAscope™ images and supplemental images were acquired using a Leica Stellaris 5 (WLL) microscope. Z-projections covering the depth of the section were captured at 63× magnification, and regions of interest were captured at 4.5 or 0.75 zoom using the same objective lens. Maximum intensity projections or individual slice overlays are represented. Signal gain was kept consistent between experimental repeats.

Cell quantification

Quantification was performed using FIJI. In all experiments, proliferation was quantified by calculating the percentage of $BrdU^+$ cells among all DAPI labeled nuclei across the entire explant.

SV sample preparation for scRNA sequencing

SV tissue samples were prepared as previously described.[30] Briefly, mice were sacrificed, and inner ears from a total of four P1 mice and four P30 mice were collected. The SV was micro-dissected from the spiral ligament and lysed in either 0.5 mg/mL trypsin at 37°C for 7 min for P1 tissue, or 400–600 units/mL accutase at 37°C for 25 min for P30 tissue. Media was gently replaced with 5% FBS in DMEM to stop lysis, and the tissue was triturated and then filtered using a 20 μm filter (pluriSelect Life Science, El Cajon, CA, United States), and the cells were kept on ice for 35 min. The cell pellet was then suspended in 50 μL of the filtered media and cell counts were performed using a Luna automated cell counter (Logos Biosystems, Annandale, VA, United States). A cell density of 1×10^6 cells/ml was used to load onto the 10× Genomics chip.

10× chromium genomics platform

Single cell captures were performed following manufacturer's recommendations on a 10x Genomics Controller device (Pleasanton, CA, United States). The number of captured cells per sample were as follows: 2259 cells, 111,122 mean reads per cell, 2422 median genes per cell from sample P1_s353n, 7790 cells, 16,260 mean reads per cell, 1859 median genes per cell from sample P1_s405n, and 5206 cells, 26,580 mean reads per cell, 1042 median genes per cell from sample P30_accu. Library preparation was performed according to the instructions in the 10× Genomics Chromium Single Cell 3′ Chip Kit V2. Libraries were sequenced on a HiSeq 1500 or Nextseq 500 instrument (Illumina, San Diego, CA, United States) and reads were subsequently processed using 10× Genomics CellRanger analytical pipeline using default settings and 10× Genomics downloadable mm10 genome. Dataset aggregation was performed using the cellranger aggr function normalizing for total number of confidently mapped reads across libraries.

Single cell RNA-sequencing data preprocessing

Quality control was conducted using the following parameters: nFeature_RNA >900 & nFeature_RNA <5000 & percent.mt < 15. Doublet detection was conducted with scDblFinder using the default parameters without clustering information. After filtering steps, we had 1973 cells for sample P1_s353n, 5724 cells for sample P1_s405n, and 2118 cells for sample P30_accu. The raw gene expression matrix was normalized using the scTransform function in Seurat,[88] and the P1 and P30 datasets were integrated after batch correction using the reciprocal principal component analysis (RPCA) method.

Dimensionality reduction and clustering

Dimensionality reduction was performed via UMAP using the first 20 principal components. Clustering was performed in smart local moving algorithm in Seurat.[89] Clusters were annotated using known published markers for each cell type.[29]

Differential expression analysis

Differential gene expression was performed in Seurat using the Wilcoxon Rank-Sum test. Average log2fc > |1|, adjusted *p*-value <0.05. Functional enrichment analysis was performed using gProfiler v. e109_e.g.,56_p17_1d3191d. Genes that were upregulated in P1 and P30 were run as separate queries per cell type, filtering out ribosomal genes. Significance threshold was set to 0.05 and multiple tests were corrected using the Bonferroni correction method.

CellChat analysis

We performed intercellular communication (ligand-receptor) analysis for P1 and P30 datasets, respectively, using CellChat[83] (v1.5.0, default parameters). Trimean algorithm was used to infer the communication network, including signaling pathway and ligand-receptor pairs information. We visualized sources and targets of each signal as Circos plots via pycirclize (https://github.com/moshi4/pyCirclize).

Trajectory analysis

We applied trajectory analysis for the fibrocyte and basal cell clusters using Slingshot v1.6.0[84] and set the fibrocyte cluster as the starting point. We visualized the expression changes (normalized values) of marker genes along with the trajectory. Supplemental analysis was performed using Slingshot, and Monocle 3,[90] setting three different starting points: intermediate cells, FB-derived cell 2, and a sub-population of fibrocytes.

QUANTIFICATION AND STATISTICAL ANALYSIS

Statistical analyses were performed using GraphPad-Prism software. For *in vitro* proliferation assays and the Wnt inhibition study, a One-way ANOVA with Tukey's Multiple Comparisons Test was performed for all experiments with the significance threshold set to $p < 0.05$. For reverse transcription quantitative real-time PCR experiments, a two-tailed Student's t test was performed for each gene between ages or conditions with the significance threshold set to $p < 0.05$. All data are represented as mean and standard error of the mean (SEM). All *n*-values presented refer to number of SV. All *p*-values are presented in figure legends.